NASA TECHNICAL NOTE

NASA TN D-2982

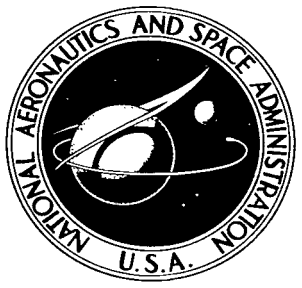

NASA TN D-2982

ENERGY ADDITION TO AN ATOMIC HYDROGEN PLASMA AT OFF-RESONANT CONDITIONS

by Richard R. Woollett

Lewis Research Center
Cleveland, Ohio

NATIONAL AERONAUTICS AND SPACE ADMINISTRATION • WASHINGTON, D. C. • SEPTEMBER 1965

ENERGY ADDITION TO AN ATOMIC HYDROGEN PLASMA AT OFF-RESONANT CONDITIONS

By Richard R. Woollett

Lewis Research Center
Cleveland, Ohio

NATIONAL AERONAUTICS AND SPACE ADMINISTRATION

For sale by the Clearinghouse for Federal Scientific and Technical Information
Springfield, Virginia 22151 – Price $2.00

ENERGY ADDITION TO AN ATOMIC HYDROGEN PLASMA AT OFF-RESONANT CONDITIONS

by Richard R. Woollett

Lewis Research Center

SUMMARY

The efficiency of energy addition to a plasma by means of a Stix coil was determined for off-resonant conditions. The results included effects of cyclotron damping and axial temperature. The coupling resonance was found to be much sharper than had been predicted previously. Additional maxima in power absorption were found at slightly higher magnetic fields. These off-resonant maxima exhibited magnitudes and breadths that made them appear well suited to plasma heating. These new maxima appeared because of a beat phenomenon between the forced and natural plasma waves.

INTRODUCTION

At present, there is considerable interest (ref. 1) in heating a magnetoplasma by the addition of electromagnetic wave energy in the neighborhood of the ion cyclotron frequency. The calculated magnitude and half breadth of the resonant absorption presented by Stix in reference 2 indicate that this technique is an efficient way to heat a plasma. However, several problems plaguing the experimentalist make it difficult to verify the theory. First, diagnostic techniques for plasmas are often of questionable value. Second, in the region of the ion cyclotron frequency, there are theoretically possible competing phenomena that could absorb the excited wave energy. An example of such a process is the particle resonance associated with atomic ions or with molecular ion-atom combinations (ref. 3). Further complications result from the shift in the resonance resulting from collisions (ref. 4). It would be helpful if theory predicted more than just the location of a resonant point. In fact, if the calculated energy addition had distinguishing features other than a simple resonant maximum, there would be strong evidence of verification from just the experimental duplication of the shape of the power curve. The present calculation of energy addition by the excitation of the natural plasma waves

(using a Stix coil, ref. 2) exhibits such distinguishing features.

The previous analysis (ref. 2) assumed a uniform, fully ionized plasma immersed in a large steady-state magnetic field. In addition, it was assumed that there were at most only a few electron-ion collisions as the ions traversed under the Stix coil. In the derivation, however, certain approximations were made in order to present the solutions in a compact form. This resulted in expressions only good for a coupling resonant condition, that is, where the wave number associated with the radiating coil system was identical to the wave number of the natural modes of the plasma. In addition, these resonant results were good over limited regions of plasma conditions. Because of these restrictions, effects associated with axial temperature and cyclotron damping were lost. The theory presented was mainly applicable to a situation where the current boundary at the coil had a pure sinusoidal wave form. In this derivation, certain questionable approximations were incorporated. This difficulty was later circumvented (ref. 5) by approaching the problem in a somewhat different manner. However, axial temperature effects, cyclotron damping, and particle energy, which are of interest in the present study, are still not covered in reference 5 for a Stix coil. In the present analysis, only a single impressed current wave shall be considered. The model used will be the same as the one used in reference 2 except that in the present case certain of the previous approximations will not be made. The equations will then be applicable at off resonance. This procedure will also extend the use of the equations to cover a continuous range of plasma conditions that include cyclotron damping and axial temperature effects when significant.

The results of the analysis are presented in the form of so-called U-factors, which represent (as in ref. 2) a nondimensional power expression. The nondimensionalizing factor is the magnetic field energy associated with a Stix coil for a no-plasma condition. The U-factors for both wave energy and the transverse kinetic energy of the particles are presented as functions of the steady-state magnetic field for the range from 4000 to 6000 gauss (the range of interest in current Lewis Research Center experiments). Calculations are presented for an atomic hydrogen plasma having the densities of 10^{11}, 10^{12}, and 10^{14} ions per cubic centimeter and having various axial temperatures between the limits of 10^{3} to 10^{5} ^{o}K. Data for coil current wave lengths of 20, 30, 40, and 50 centimeters are also presented. A numerical comparison is also made between the various dispersion relations involved in the analysis.

SYMBOLS

A atomic number of ion

$A_{\pm}$ defined by eq. (4)

a_m, b_m	coefficients of Fourier-Bessel expansion for electric field
$\tilde{B}$	nondimensional amplitude of perturbation magnetic field (perturbation field in G divided by B_0)
B_0	zero-order axial magnetic field strength, G
$B_0(res)$	value of magnetic field for which coupling resonance of ref. 2 occurs for a given frequency, G
c	speed of light, cm/sec
$\tilde{E}$	amplitude of electric field, esu/B_0
$\mathscr{E}_i$	kinetic energy of ions, eq. (10a)
$\mathscr{G}$	defined by eq. (32)
$I_n(z)$	modified Bessel function of first kind and order n (ref. 6)
$I_\pm$	defined by eqs. (5a) and (5b)
$J_n(z)$	Bessel functions of order n (ref. 6)
$\tilde{j}^*$	amplitude of sheet current, (abs amp/cm)$(4\pi/B_0)$
$K_n(z)$	modified Bessel function of second kind and order n (ref. 6)
k	wave number, rad/cm
$\mathscr{k}$	Boltzmann's constant
L	nondimensional coil length, $l\omega_{ci}/c$
l	coil length, cm
M	defined by eq. (25)
m	mass of ions, g
N	number of wavelengths per coil length (N = 2 for all calculations)
n	particle density, ions/cm^3
P	average power transferred from coil to plasma for given sinusoidal coil current, ergs/sec
P_D	peak radio-frequency magnetic field energy in a vacuum (times ω), defined by eq. (18)
$p_\pm$	$(1 \pm \Omega)(\kappa s_0)^{-1}$
Q	storage factor of coil
R	nondimensional radius, $r\omega_{ci}/c$

$\mathcal{R},\mathcal{S}$	defined by eqs. (19b) and (19d)
r	radius, cm
r_0	plasma radius, cm
$S(\delta)$	defined by eq. (35a)
S_0, S_1	defined by eq. (35a)
s_0	nondimensional axial velocity, $(2kT_i/mc^2)^{1/2}$
T	nondimensional time, $t\omega_{ci}$
T_i	axial temperature of plasma
T_0	time ion starts path under coil
t	time, sec
U	power absorption factor (U-factor), P/P_D
U_0, U_1	real part of Bessel function of orders 0 and 1, respectively
V_0, V_1	imaginary part of Bessel function of orders 0 and 1, respectively
W	defined by eq. (12)
Z	nondimensional axial distance, $z\frac{\omega_{ci}}{c}$
Z_i	charge number of ion
Z_0	location at end of coil
z	axial coordinate, cm
$\hat{z}$	axial unit vector
α	$4\pi nmc^2/B_0^2$
β	defined by eq. (8b)
β_m	defined by eq. (31)
γ	defined by eq. (33)
δ	defined by eq. (35b)
ϵ	defined by eq. (26a)
ζ	defined by eq. (26b)
η	defined by eqs. (22), (23), and (24)
κ	nondimensional axial wave number, $k\frac{c}{\omega_{ci}}$
κ_D	$(\kappa^2 - \Omega_D^2)^{1/2}$

λ	axial wavelength, cm
μ	defined by eq. (8b)
ν	nondimensional radial wave number
ν_0	real part of ν
ν_1	imaginary part of ν
ξ	defined by eq. (26b)
ρ	defined by eq. (8b)
σ_1	axial conductivity, eq. (2)
σ_2	transverse conductivity, eq. (3)
τ	defined by eq. (8b)
Υ, Φ, Ψ	defined on pp. 19 and 20
φ	defined by eq. (16b)
Ω	nondimensional frequency, ω/ω_{ci}
Ω(res)	frequency for B_0(res)
Ω_D	nondimensional frequency ω/ω_{ci}, which originates from the vacuum displacement current term in Maxwell's equation
ω	frequency, radians/sec
ω_{ci}	ion cyclotron frequency, $B_0 e/mc$

Subscripts:

c	cold plasma
m	various natural modes
p	particle
r, θ, z	cylindrical coordinates
w	wave
x, y, z	rectangular coordinates
$\perp$	component of vector perpendicular to the z-axis

Superscript:

~	amplitude factor of the perturbation $e^{i(kz+\omega t)}$
'	designates derivative of Bessel function with respect to its argument

THEORY

Dispersion Relation

The mathematical model used to develop the equations to determine the power transfer is essentially the same as the model used by Stix. Both models used the following set of assumptions:

(1) The plasma is fully ionized.

(2) The I^2R losses, gravity, viscosity, and electron inertia are neglected.

(3) The ion temperature is nonisotropic, that is, zero in the transverse direction.

(4) The distribution of the axial velocity of the ions is Maxwellian.

(5) All oscillations are periodic in axial distance and in time (i.e., contain the factor $e^{i(kz+\omega t)}$).

(6) The perturbation velocities are small amplitude oscillations perpendicular to a steady-state magnetic field.

(7) Perturbations of the electron and ion axial velocities are ignored. Consequently, the derivations will follow very closely those presented in reference 2.

The essential character of electromagnetic wave propagation through a plasma is represented in the dispersion relation. This expression is entirely independent of plasma size and depends only on the various transport properties of the gas. Since the dispersion relation is completely dependent on plasma currents, which in turn depend on particle (ion and electron) velocity, the initial step in the derivation of the equations is to obtain relations for the various particle velocities. This is done by first dividing the plasma into a massless electron fluid and into constituent streams of ions. Each constituent stream consists of those ions of the Maxwellian distribution that have the same axial velocity. The expression for the average transverse ion velocity is now obtained by solving the equation of motion of each constituent stream and adding the various streams together. By a similar technique it can be shown that the electron velocity is comprised of two parts - one originating from the free motion along the steady-state magnetic field and the other from an $E \times B$ drift motion. With these expressions for the average velocity of the particles under the coil, a plasma current may be derived, which when used with Maxwell's equation results in the following wave equation:

$$\left[\nabla \times (\nabla \times \tilde{E}) - \Omega_D^2 \tilde{E} = \sigma_1 \tilde{E} + i\sigma_2 \tilde{E} \times \hat{z}\right]_\perp \tag{1}$$

$$\sigma_1 \equiv \alpha(I_+ + I_- - 1) + i\alpha(A_+ - A_-) \tag{2}$$

$$\sigma_2 \equiv \alpha(\Omega + I_+ - I_-) + i\alpha(A_+ + A_-) \tag{3}$$

Equation (1) is the same as equation (7) of reference 2 except for the retention of the displacement current term $\Omega_D^2 \tilde{E}$. Including the displacement currents extends the range of validity of the solutions to very high frequencies, such as those corresponding to ion cyclotron resonance at high magnetic fields. The quantity Ω_D that appears throughout the report is identical to Ω but is given the subscript D when it appears in terms that originate from the displacement currents. The expressions used for A_+ and A_- are the long-time asymptotic forms presented in reference 2, which are equal to

$$A_\pm = \frac{\lambda B_0 Z_i}{9.47 A^{1/2} T_i^{1/2}} e^{-p_\pm^2} \tag{4}$$

The quantities $I_\pm$ can be expressed in the form

$$I_\pm = \frac{1}{\kappa s_0} e^{-p_\pm^2} \int_0^{p_\pm} e^{x^2} dx \tag{5a}$$

For $p_\pm \geq 12$, equation (5a) is represented to good accuracy by

$$I_\pm = \frac{1}{2p_\pm \kappa s_0} \left(1 + \frac{1}{2p_\pm^2} + \frac{3}{2p_\pm^4} \right) \tag{5b}$$

Equation (5b) is an asymptotic form of equation (5a) and is obtained by evaluating $e^{-y^2} \int_0^y e^{x^2} dx$ for large arguments by L'Hospital rule. For $p_\pm = 12$, the difference in the two expressions is less than one in the seventh place. This accuracy is the same order as that involved in the evaluation of equation (5a) itself. To evaluate equation (5a), a table obtained from reference 7 was used.

The solution of equation (1) shows that, for a uniform axially symmetric plasma where σ_1 and σ_2 are independent of position, $\tilde{E}_r$ and $\tilde{E}_\theta$ vary as the unmodified Bessel function of the first kind and of the first order. The radial wave number ν that appears in the Bessel function $J_1(\nu R)$ can be written as

$$\nu^2 = \frac{(\sigma_1 - \kappa_D^2)^2 - \sigma_2^2}{\sigma_1 - \kappa_D^2} \tag{6}$$

where

$$\kappa_D^2 = \kappa^2 - \Omega_D^2$$

This is the dispersion relation for the propagation of an electromagnetic wave through the plasma model described previously. It includes effects of cyclotron damping and vacuum displacement currents.

To determine the real and imaginary parts of ν from equation (6), let

$$\nu = \nu_0 + i\nu_1$$

Then

$$\nu^2 = (\nu_0 + i\nu_1)^2 = (\nu_0^2 - \nu_1^2) + 2\nu_0\nu_1 i$$

Consequently,

$$\text{Re } \nu^2 = \nu_0^2 - \nu_1^2$$

$$\text{Im } \nu^2 = 2\nu_0\nu_1$$

Expressions for ν_0 and ν_1 can readily be obtained from these equations as functions of Re ν^2 and Im ν^2, which in turn can be obtained by substituting equations (2) and (3) into equation (6) and by collecting the real and imaginary parts of the resulting expression. This results in

$$\text{Re } \nu^2 = \frac{\mu\left[(\mu^2 - \beta^2) - (\tau^2 - \rho^2)\right] + 2\tau\left[\mu\tau - \beta\rho\right]}{\mu^2 + \tau^2} \tag{7}$$

$$\text{Im } \nu^2 = \frac{\tau\left[(\tau^2 - \rho^2) - (\mu^2 - \beta^2)\right] + 2\mu\left[\mu\tau - \beta\rho\right]}{\mu^2 + \tau^2} \tag{8a}$$

where

$$\left.\begin{aligned} \mu &= \text{Re}\ \sigma_1 - \kappa_D^2 \\ \beta &= \text{Re}\ \sigma_2 \\ \tau &= \text{Im}\ \sigma_1 \\ \rho &= \text{Im}\ \sigma_2 \end{aligned}\right\} \tag{8b}$$

With the previous expressions for ν_0 and ν_1 it is possible to obtain the radial distribution of E_θ and E_r for a forced axial variation of the electric fields. From these distributions it is possible to calculate the power absorbed by the plasma.

Power Absorption U-Factor

There are several ways in which the plasma can absorb energy. One of these is by means of the kinetic energy of the particles involved, and the other is by a cooperative effect of the ions and electrons such that the electric and magnetic field intensities within the plasma increase above the vacuum values. The two sets of calculations to determine the absorbed energy start from two different and not necessarily self-consistent models.

So far the relations developed do not involve any plasma boundary conditions. When energy calculations are made, however, boundary conditions have to be considered. For the present calculations, energy is radiated from a Stix coil and is absorbed by the plasma. It is then propagated out from under the coil either by a plasma wave or through the kinetic energy tied up with the ion motion. The results are presented in terms of a relative power efficiency, called the U-factor, and defined by

$$U = \frac{P}{P_D} \tag{9}$$

where P is the average power transferred from the coil to the plasma for a given sinusoidal coil current, and P_D is the product of ω and the peak radio-frequency magnetic energy stored in the field of the coil in the absence of a plasma. Actually there are other factors (see ref. 2) involved in determining an overall efficiency, but they all represent power losses originating from the geometry of the coil system. These additional factors are neglected, since the primary concern herein is the ability of a plasma

to absorb power, which is solely dependent on the U-factor. If the plasma fills the volume under the coil, the overall efficiency (ratio of power input to the plasma to the total power used) is $QU/(1 + QU)$ where Q is the vacuum Q of the coil.

Power absorption by particle resonance (U_p). - Considered first is the energy absorbed by the particles themselves. It has been shown (ref. 2) that if the transverse energy of an ion averaged over an oscillatory cycle is further averaged over a Maxwellian distribution of axial velocities, the resulting average energy as a function of time (ref. 2) is

$$\mathscr{E}_i = mc^2 \left\{ \left[F_0 + (T - T_0) \frac{A_+}{2} \right] |\tilde{E}_x + i\tilde{E}_y|^2 + \left[F_0 + (T - T_0) \frac{A_-}{2} \right] |\tilde{E}_x - i\tilde{E}_y|^2 \right\} \tag{10a}$$

where F_0 is a term independent of time. The power associated with such a phenomenon can be obtained by taking the time derivative of this energy:

$$P_p = \omega_{ci} n \int_{Vol} \frac{d(\mathscr{E}_i)}{dT} \, dV \tag{10b}$$

where the integration extends over the volume under the Stix coil. When equation (10a) is substituted into equation (10b)

$$P_p = \frac{\omega_{ci} nmc^2}{2} \left(A_+ \int |\tilde{E}_x + i\tilde{E}_y|^2 \, dV + A_- \int |\tilde{E}_x - i\tilde{E}_y|^2 \, dV \right)$$

But

$$\tilde{E}_x \pm i\tilde{E}_y = i\tilde{E}_\theta \left(\frac{\tilde{E}_r}{i\tilde{E}_\theta} \pm 1 \right)$$

so that

$$P_p = \frac{\pi l \omega_{ci} nmc^2}{2} \left(\left| 1 + \frac{\tilde{E}_r}{i\tilde{E}_\theta} \right|^2 A_+ + \left| 1 - \frac{\tilde{E}_r}{i\tilde{E}_\theta} \right|^2 A_- \right) \int_0^r r \left| \tilde{E}_\theta \right|^2 dr \tag{11}$$

where

$$l = N\lambda$$

The solution of equation (1) with the boundary conditions for an infinitely long cylindrical plasma bounded by an azimuthal sheet current having a sinusoidal axial variation, that is, $\tilde{j}^* e^{i(\kappa z + \omega t)}$, yields

$$\tilde{E}_\theta = W J_1(\nu R)$$

where

$$W = \frac{\tilde{j}^* \Omega i R_0}{\left[\nu R_0 \frac{J_1'(\nu R_0)}{J_1(\nu R_0)} - \kappa_D R_0 \frac{K_1'(\kappa_D R_0)}{K_1(\kappa_D R_0)} \right] J_1(\nu R_0)} \tag{12}$$

This expression can be used with real, imaginary, or complex ν. The integral in equation (11) now becomes

$$\int_0^r r \left| \tilde{E}_\theta \right|^2 dr = |W|^2 \int_0^r r \left| J_1(\nu R) \right|^2 dr \tag{13}$$

When ν is real, equation (13) yields

$$\int_0^{R_0} R J_1^2(\nu R) dR = \frac{R_0^2}{2} \left[J_1'^2(\nu R_0) + \left(1 - \frac{1}{\nu^2 R_0^2} \right) J_1^2(\nu R_0) \right] \tag{14}$$

When ν is imaginary, the integral in equation (13) may be evaluated by setting $J_1(i\nu_1 R_0) = iI_1(\nu_1 R_0)$. The result is

$$\int_0^{R_0} R|E_\theta|^2\,dR \propto \int_0^{R_0} R|J_1(i\nu_1 R_0)|^2\,dR = \int_0^{R_0} RI_1^2(\nu_1 R_0)dR$$

$$= -\frac{R_0^2}{2}\frac{I_1^2(\nu_1 R_0)}{\nu_1^2 R_0^2}\left[(\nu_1 R_0)^2\frac{I_0^2(\nu_1 R_0)}{I_1^2(\nu_1 R_0)} - 2(\nu_1 R_0)\frac{I_0(\nu_1 R_0)}{I_1(\nu_1 R_0)} - (\nu_1 R_0)^2\right] \tag{15}$$

The remaining case for ν complex is somewhat more involved since $J_1(\nu R)$ itself is a complex number. The integral can be expressed as

$$\int_0^{R_0} R|J_1|^2\,dr = -\frac{R}{2|\nu|}\left\{\left[U_1(\nu R_0)U_0(\nu R_0) + V_1(\nu R_0)V_0(\nu R_0)\right]\sec\varphi\right.$$

$$\left. - \left[U_0(\nu R_0)V_1(\nu R_0) - U_1(\nu R_0)V_0(\nu R_0)\right]\csc\varphi\right\} \tag{16a}$$

where

$$\left.\begin{aligned} \varphi &= \arctan\frac{\nu_1}{\nu_0} \\ |\nu| &= (\nu_0^2 + \nu_1^2)^{1/2} \\ J_0(\nu R_0) &= U_0(\nu R_0) + iV_0(\nu R_0) \\ J_1(\nu R_0) &= U_1(\nu R_0) + iV_1(\nu R_0) \end{aligned}\right\} \tag{16b}$$

The term in equation (11) involving the ratio of electric fields may be evaluated from the $\hat{\mathbf{r}}$ component of the wave equation (eq. (1)). Thus,

$$\frac{\tilde{E}_r}{i\tilde{E}_\theta} = \frac{\sigma_2}{\kappa_D^2 - \sigma_1} \tag{17}$$

Consequently,

$$\left| 1 \pm \frac{\tilde{E}_r}{i\tilde{E}_\theta} \right|^2 = \frac{(\mu \mp \beta)^2 + (\tau \mp \rho)^2}{\mu^2 + \tau^2}$$

where μ, β, τ, and ρ are defined by equations (8b).

Before the U-factor can be obtained, an expression must be derived for the quantity P_D (eq. (9)). This expression can be given as

$$P_D = \frac{\omega}{16\pi} \int_{Vol} B_0^2 |\tilde{B}|^2 \, dV \tag{18}$$

where the integration is from zero to infinity radially and is bounded by the ends of the coil axially. The magnetic field components under an ideal coil are given by

$$\left.\begin{aligned} \tilde{B}_r &= \Re \frac{\kappa}{\Omega} I_1(\kappa_D R) \\ \tilde{B}_\theta &= 0 \\ \tilde{B}_z &= i\Re \frac{\kappa_D}{\Omega} I_0(\kappa_D R) \end{aligned}\right\} \tag{19a}$$

where

$$\Re = i\tilde{j}^* \Omega R_0 K_1(\kappa_D R_0) \tag{19b}$$

Outside of the ideal coil they are given by

$$\left.\begin{aligned} \tilde{B}_r &= \mathcal{S} \frac{\kappa}{\Omega} K_1(\kappa_D R) \\ \tilde{B}_\theta &= 0 \\ \tilde{B}_z &= -i\mathcal{S} \frac{\kappa_D}{\Omega} K_0(\kappa_D R) \end{aligned}\right\} \tag{19c}$$

where

$$\mathcal{S} = \mathcal{R}\,\frac{I_1(\kappa_D R_0)}{K_1(\kappa_D R_0)} \tag{19d}$$

Adding all the field energies present results in

$$P_D = \frac{\omega}{8}\,N\lambda B_0^2 \tilde{j}^{*2} r_0^2 K_1(\kappa_D R_0) I_1(\kappa_D R_0) \tag{20}$$

When equations (11) to (14) and (20) are substituted into $U_p = P_p/P_D$,

$$U_p = \frac{M\Omega\eta}{2K_1(\kappa_D R_0) I_1(\kappa_D R_0)} \tag{21}$$

where

$$\eta = \frac{\left[\nu_0 R_0 \dfrac{J_0(\nu_0 R_0)}{J_1(\nu_0 R_0)}\right]^2 - 2\nu_0 R_0 \dfrac{J_0(\nu_0 R_0)}{J_1(\nu_0 R_0)} + \nu_0^2 R_0^2}{\nu_0^2 \left[\nu_0 R_0 \dfrac{J_0(\nu_0 R_0)}{J_1(\nu_0 R_0)} + \kappa_D R_0 \dfrac{K_0(\kappa_D R_0)}{K_1(\kappa_D R_0)}\right]^2} \quad \text{for } \nu_1 = 0 \tag{22}$$

$$\eta = \frac{\left[\nu_1 R_0 \dfrac{I_0(\nu_1 R_0)}{I_1(\nu_1 R_0)}\right]^2 - 2\nu_1 R_0 \dfrac{I_0(\nu_1 R_0)}{I_1(\nu_1 R_0)} - (\nu_1 R_0)^2}{\nu_1^2 \left[\nu_1 R_0 \dfrac{I_0(\nu_1 R_0)}{I_1(\nu_1 R_0)} + \kappa_D R_0 \dfrac{K_0(\kappa_D R_0)}{K_1(\kappa_D R_0)}\right]^2} \quad \text{for } \nu_0 = 0 \tag{23}$$

$$\eta = R_0 \left\{ \frac{\left[U_1(\nu R_0)U_0(\nu R_0) + V_1(\nu R_0)V_0(\nu R_0)\right]\sec\varphi - \left[U_0(\nu R_0)V_1(\nu R_0) - U_1(\nu R_0)V_0(\nu R_0)\right]\csc\varphi}{\epsilon\left[\nu_0^2 + \nu_1^2\right]^{1/2}\left[U_1^2(\nu R_0) + V_1^2(\nu R_0)\right]} \right\}$$

for ν complex (24)

$$M = \alpha\left\{\left|1 + \frac{\tilde{E}_r}{i\tilde{E}_\theta}\right|^2 A_+ + \left|1 - \frac{\tilde{E}_r}{i\tilde{E}_\theta}\right|^2 A_-\right\} \tag{25}$$

$$\epsilon = \left[\frac{R_0\left[\xi U_1(\nu R_0) + \xi V_1(\nu R_0)\right]}{U_1^2(\nu R_0) + V_1^2(\nu R_0)} + \kappa_D R_0 \frac{K_0(\kappa_D R_0)}{K_1(\kappa_D R_0)}\right]^2 + \left[\frac{R_0\left[\xi U_1(\nu R_0) - \xi V_1(\nu R_0)\right]}{U_1^2(\nu R_0) + V_1^2(\nu R_0)}\right]^2 \tag{26a}$$

$$\left.\begin{aligned} \zeta &= \nu_0 U_0(\nu R_0) - \nu_1 V_0(\nu R_0) \\ \xi &= \nu_1 U_0(\nu R_0) + \nu_0 V_0(\nu R_0) \end{aligned}\right\} \tag{26b}$$

With equations (21) to (26a) it is possible to calculate the U-factor due to adding power to a plasma by means of the kinetic energy of the ions present.

Power absorption by means of waves (U_w). - Power absorption by means of waves is by far the more important of the two phenomena being considered herein, because the magnitude of the U-factor for wave absorption is generally considerably larger except perhaps at the coupling resonant condition. This wave energy absorption is accomplished by increasing the wave amplitude and changing the phase angle. Before proceeding with the analytical formulation of the problem, the boundary conditions must be explicitly stated since they play a more integral part in the derivation of wave energy than in particle energy. It is considered that the region of the plasma which responds to the forced radio frequency wave lies inside a "box" beneath the Stix coil. This plasma box is bounded on the left and right, outside of the Stix coil, by a cylindrical plasma that extends to infinity and has a radius r_0 equal to that of the coil. The plasma box is also bounded by the coil itself. The solutions for the plasma box and the infinite plasma outside the coil are joined by making the wave amplitudes continuous at the boundary. Outside of the coil, the wave motion is assumed to be a natural mode of oscillation of a cylindrically bounded plasma in which the wave amplitude is constant. In the left hand region, the amplitude of a right running wave is zero. The right running wave squirts out the right end of the coil and propagates axially to infinity (ref. 2). An analogous phenomenon occurs with the left running wave. Underneath the exciting coil, it has been assumed that the forced plasma wave is equal to that generated by a Stix coil of infinite length. The forced wave, that is, $J_1(\nu R)$, in the plasma box under the Stix coil can be Fourier decomposed into an infinite series of $J_1(\nu_m R)$; that is,

$$J_1(\nu R) = \sum a_m J_1(\nu_m R)$$

where ν_m is the radial wave number for the m^{th} radial mode of oscillation of the free cylindrical plasma. The forced electric field is given by

$$\tilde{E}_\theta e^{i(\kappa Z+\Omega T)} = W J_1(\nu R) e^{i(\kappa Z+\Omega T)}$$

Consequently,

$$\tilde{E}_\theta = \sum_{m=1}^{\infty} W a_m J_1(\nu_m R)$$

The natural mode relation used was obtained from expressions previously developed (ref. 8) for cold collisionless plasmas (for which no cyclotron damping occurs). For a given Ω, B_0, and n these natural modes can be obtained from the simultaneous solution of the following two equations (ref. 8):

$$\nu_c^2 = \frac{-\Omega^4\alpha^2 + \Omega^2\left[2\alpha + \left(\kappa_c^2 - \Omega_D^2\right)\right]\left(\kappa_c^2 - \Omega_D^2\right) - \left(\kappa_c^2 - \Omega_D^2\right)^2}{-\Omega^2\left[\alpha + \left(\kappa_c^2 - \Omega_D^2\right)\right] + \left(\kappa_c^2 - \Omega_D^2\right)} \tag{27}$$

and

$$\nu_c R_0 \frac{J_0(\nu_c R_0)}{J_1(\nu_c R_0)} = -\left(\kappa_c^2 - \Omega_D^2\right)^{1/2} R_0 \frac{K_0\left(\left(\kappa_c^2 - \Omega_D^2\right)^{1/2} R_0\right)}{K_1\left(\left(\kappa_c^2 - \Omega_D^2\right)^{1/2} R_0\right)} \tag{28}$$

Equation (27) is the dispersion relation for a cylindrically symmetric plasma where the perturbations have the form $J_1(\nu_c R)e^{i(\kappa_c Z+\Omega T)}$. Equation (28) is obtained from the wave equation and the "boundary condition" for a vacuum boundary of a plasma located at $R = R_0$. The azimuthal electric field, along with its associated magnetic field, were both assumed continuous across the boundary. In the derivation of equations (27) and (28), the axial electric field was set equal to zero (negligible electron mass). It is not a particularly straightforward calculation to find a solution which is designated ν_m and κ_m from these expressions. The technique used herein is outlined in appendix A.

Once the values of the wave numbers associated with the natural modes of plasma

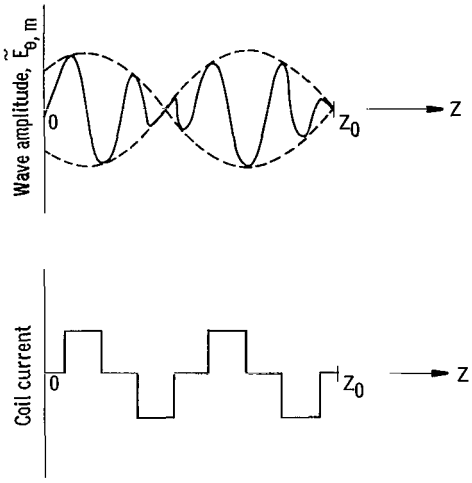

Figure 1. - Schematic of spatial variation of wave amplitude and coil current.

oscillation have been determined, an expression for the electric fields under the coil can be derived. In order to satisfy the boundary conditions existing on each end of the coil, a natural mode wave must be added to the forced disturbance. This is analogous to adding a complementary solution of a differential equation to its particular solution. The electric field under the coil can be represented by

$$\tilde{E}_\theta e^{i(\kappa Z+\Omega T)} = \sum Wa_m J_1(\nu_m R) e^{i(\kappa Z+\Omega T)} + \sum b_m J_1(\nu_m R) e^{i(\kappa_m Z+\Omega T)} \tag{29}$$

where the b_m's are coefficients to be determined by the boundary conditions. (Only a term equivalent to the first series on the right hand side of eq. (29) was required for the fields in the particle model.) The boundary condition requires that the electric field for each left running radial mode vanishes at the right end of the coil, that is, at $Z = Z_0$ (see fig. 1). This results in

$$Wa_m e^{i\kappa Z_0} + b_m e^{i\kappa_m Z_0} = 0$$

and

$$b_m = -Wa_m e^{i(\kappa-\kappa_m)Z_0}$$

Consequently, equation (29) becomes

$$\tilde{E}_\theta e^{i(\kappa Z+\Omega T)} = \sum \frac{\beta_m J_1(\nu_m R)}{\nu^2 - \nu_m^2}\left[1 - e^{-i(\kappa-\kappa_m)(Z-Z_0)}\right] e^{i(\kappa Z+\Omega T)} \tag{30}$$

If it is assumed that the terms of the Fourier Bessel expansion of $J_1(\nu R)$ are all orthogonal, then the following expression for β_m can be developed by normal techniques:

$$\beta_m = \frac{2i\Omega\tilde{j}^*\gamma}{R_0\left[1 + (\mathcal{G}^2 - 1)(\nu_m R_0)^{-2}\right]J_1(\nu_m R_0)} \tag{31}$$

where

$$\mathcal{G} = \frac{-\left(\kappa_m^2 - \Omega_D^2\right)^{1/2} R_0 K_1'\left(\left(\kappa_m^2 - \Omega_D^2\right)^{1/2} R_0\right)}{K_1\left(\left(\kappa_m^2 - \Omega_D^2\right)^{1/2} R_0\right)} \tag{32}$$

and

$$\gamma = \frac{\nu R_0 \dfrac{J_0(\nu R_0)}{J_1(\nu R_0)} + \left(\kappa_m^2 - \Omega_D^2\right)^{1/2} R_0 \dfrac{K_0\left(\left(\kappa_m^2 - \Omega_D^2\right)^{1/2} R_0\right)}{K_1\left(\left(\kappa_m^2 - \Omega_D^2\right)^{1/2} R_0\right)}}{\nu R_0 \dfrac{J_0(\nu R_0)}{J_1(\nu R_0)} + \kappa_D R_0 \dfrac{K_0(\kappa_D R_0)}{K_1(\kappa_D R_0)}} \tag{33}$$

This expression for β_m varies somewhat from that of reference 2 because of the inclusion of several terms that were dropped in that reference. The assumption that all the $J_1(\nu_m R)$'s are orthogonal, of course, is incorrect. However, calculations have been made of the greatest possible error evolving from this approximation. The results indicate that the error in the various coefficients of the expansion is less than 1 percent. The expression for γ given by equation (33) can still be used when ν is complex. It can be noticed that when ν is either real or imaginary, γ is real; when ν is complex, γ is complex. Equations (30) to (33) represent the electric field of a particular plasma mode set up by distributed currents within the plasma. If this field is evaluated at the coil radius, total power input into the plasma may be obtained by integrating over the surface of the plasma boundary the product of the electric field and the current required to create it. When this operation is performed, there is an expression for the average power going into the m^{th} radial mode $(P_w)_m$:

$$(P_w)_m = \mathrm{Re}\left[\frac{B_0^2 c^3}{8\omega_{ci}^2}(i)\beta_m \tilde{j}^* L^2 \frac{R_0(\kappa - \kappa_m)J_1(\nu_m R_0)}{\nu^2 - \nu_m^2} S(\delta)\right] \tag{34}$$

where

$$S(\delta) \equiv \frac{1 - \cos 2\delta + i(2\delta - \sin 2\delta)}{2\delta^2} = S_0 + iS_1 \tag{35a}$$

and

$$\delta \equiv (\kappa - \kappa_m)L/2 \tag{35b}$$

It may be noticed that equations (34) and (35a) are identical to equations (22) and (23) of reference 2. The region of Ω in which damping is important will be shown to be extremely small and centered about the point $\Omega = 1$. If there is no damping present, only the real part of $S(\delta)$ enters in the expression for real power; the imaginary term consequently represents the reactive power. The previous expression for power has the units of ergs per second. If the resistive power (eq. (34)) is nondimensionalized with respect to the same expression (eq. (20)) used with the particle power, then the U-factor for the resistive wave, m^{th} mode, is

$$(U_w)_m = - \frac{4L(\kappa - \kappa_m)\Upsilon}{\left(\nu_0^2 - \nu_1^2 - \nu_m^2\right)^2 + 4\nu_0^2\nu_1^2} \Bigg/ 2R_0^2\left[1 + \frac{\mathcal{G}^2 - 1}{(\nu_m R_0)^2}\right]K_1(\kappa_D R_0)I_1(\kappa_D R_0) \tag{36}$$

For ν_0 or $\nu_1 = 0$,

$$\Upsilon = \left[S_0(\nu_0^2 - \nu_1^2 - \nu_m^2) + 2\nu_0\nu_1 S_1\right]\gamma$$

For ν complex,

$$\Upsilon = (\mathrm{Re}\ \Psi)\left[S_0(\nu_0^2 - \nu_1^2 - \nu_m^2) + 2(\nu_0\nu_1 S_1)\right] - (\mathrm{Im}\ \Psi)\left[S_1(\nu_0^2 - \nu_1^2 - \nu_m^2) - 2\nu_0\nu_1 S_0\right]$$

where

$$\text{Re } \Psi = \frac{\left[\text{Re } \Phi + f(\kappa_m)\right]\left[\text{Re } \Phi + f(\kappa)\right] + (\text{Im } \Phi)^2}{\left[\text{Re } \Phi + f(\kappa)\right]^2 + (\text{Im } \Phi)^2}$$

$$\text{Im } \Psi = \frac{\text{Im } \Phi\left[f(\kappa) - f(\kappa_m)\right]}{\left[\text{Re } \Phi + f(\kappa)\right]^2 + (\text{Im } \Phi)^2}$$

$$\text{Re } \Phi = \frac{R_0\left[U_1(\nu_0 U_0 - \nu_1 V_0) + V_1(\nu_1 U_0 + \nu_0 V_0)\right]}{U_1^2 + V_1^2}$$

$$\text{Im } \Phi = \frac{R_0\left[U_1(\nu_1 U_0 + \nu_0 V_0) - V_1(\nu_0 U_0 - \nu_1 V_0)\right]}{U_1^2 + V_1^2}$$

$$f(x) = \left(x^2 - \Omega_D^2\right)^{1/2} R_0 \frac{K_0\left(\left(x^2 - \Omega_D^2\right)^{1/2} R_0\right)}{K_1\left(\left(x^2 - \Omega_D^2\right)^{1/2} R_0\right)}$$

and where the U's and V's are defined by equation (16b).

All the relations required to determine the efficiency of adding energy to a plasma by means of the wave energy and the particle energy have now been presented. The expressions do not require that calculations be made at a natural wave resonance condition. Calculations were performed at various ion densities, frequencies, axial ion temperatures, and plasma radii. They were performed for a fully ionized atomic hydrogen gas.

RESULTS

The results will be discussed in four sections, each of which is fairly independent of the other. The first section, Wave Number, examines the natural modes of a cylindrical plasma for a range of plasma radii, wave frequencies, and particle densities. The second section, Absorption Characteristics, discusses, without reference to the actual magnitudes of the parameters involved, the trends of energy addition to the plasma. The third and fourth sections, "Wave absorption (U-factor)" and "Particle absorption (U-factor)," present the numerical results of the energy addition calculations.

Wave Number

Since the natural modes play an integral part in the development of the theory, it is of interest to examine their characteristics in detail before the results of the U-factor calculations are presented. The natural modes used herein were obtained from the solution of the dispersion relation (eq. (27)) and the equation obtained from the boundary condition (eq. (28)). The analysis technique used is presented in appendix A. A graphic presentation of the solution is given in figure 2. Moreover, various trends can be predicted from these figures. The dispersion relation and boundary condition solutions are presented as solid and dotted curves, respectively. The natural mode, obtained from the simultaneous solution of equations (27) and (28) are consequently represented by the coordinates of the intercepts of the two curves. In figure 2(a) the boundary condition is shown for the first three modes of a plasma with a 5-centimeter radius. In figure 2(b) the boundary condition is presented for the first mode of plasmas of various radii. Qualitatively, a higher mode can be compared to the first mode for a plasma of smaller radius. It can be noticed from these figures that the axial wave number κ_c is practically independent of the boundary condition while the radial wave number ν_c is practically independent of the dispersion relation. In other words, the plasma radius and mode determine the radial wave number while the frequency determines the axial wave number. The magnetic field value of 4200 gauss in these figures is typical of the values used in the Lewis plasma heating experiments (ref. 1).

A summary of the fundamental mode wave numbers presented as a function of radius is shown in figures 3(a) and (b). The insensitivity of κ_m to radius is again demonstrated, as is the dependence of the radial wave number ν_m. Effects of plasma density can be seen by comparing the two figures (note that the scale for κ_m is not the same on these two figures).

An upper limit to the radial wave number ν_m can be found. If the boundary were an infinitely conducting surface rather than a vacuum, the radial modes would be determined by the zeros of $J_1(\nu R)$. The resulting wave numbers would be larger than the ones associated with the vacuum boundary. Moreover, the actual value of the first zero is less than $\frac{5}{4}\frac{\pi}{R}$. This upper limit to the first radial mode is included in figure 3 for comparison.

The dispersion relations presented in figures 2 and 3 however, do not include any cyclotron damping effects. An indication of when these effects are significant can be obtained by comparing the real part of ν^2, that is, $\nu_0^2 - \nu_1^2$, from equation (6) with ν^2 from equation (27). The dispersion relation of the cyclotron damped wave is plotted in figure 4. By comparing figure 2 with figure 4, it can be seen that although the equations (27) and (6) start from different physical models (the latter admits a Maxwellian distribution of axial velocity and the former does not), the calculated results are very nearly

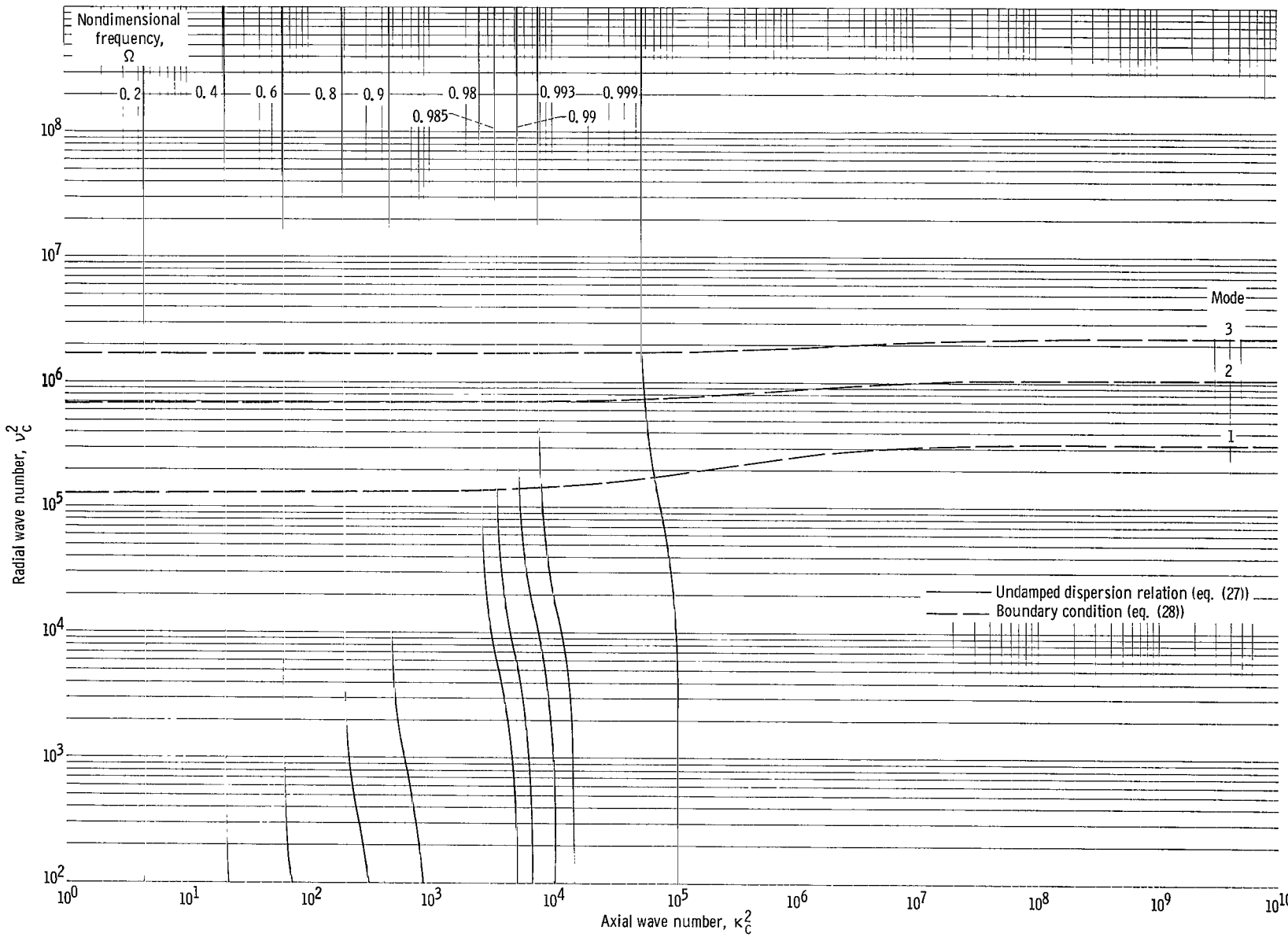

(a) Plasma radius, 5 centimeters; modes 1, 2, and 3.

Figure 2. - Graphical solution for wave numbers of natural modes. Particle density, 10^{11} ions per cubic centimeter; magnetic field, 4.2×10^3 gauss.

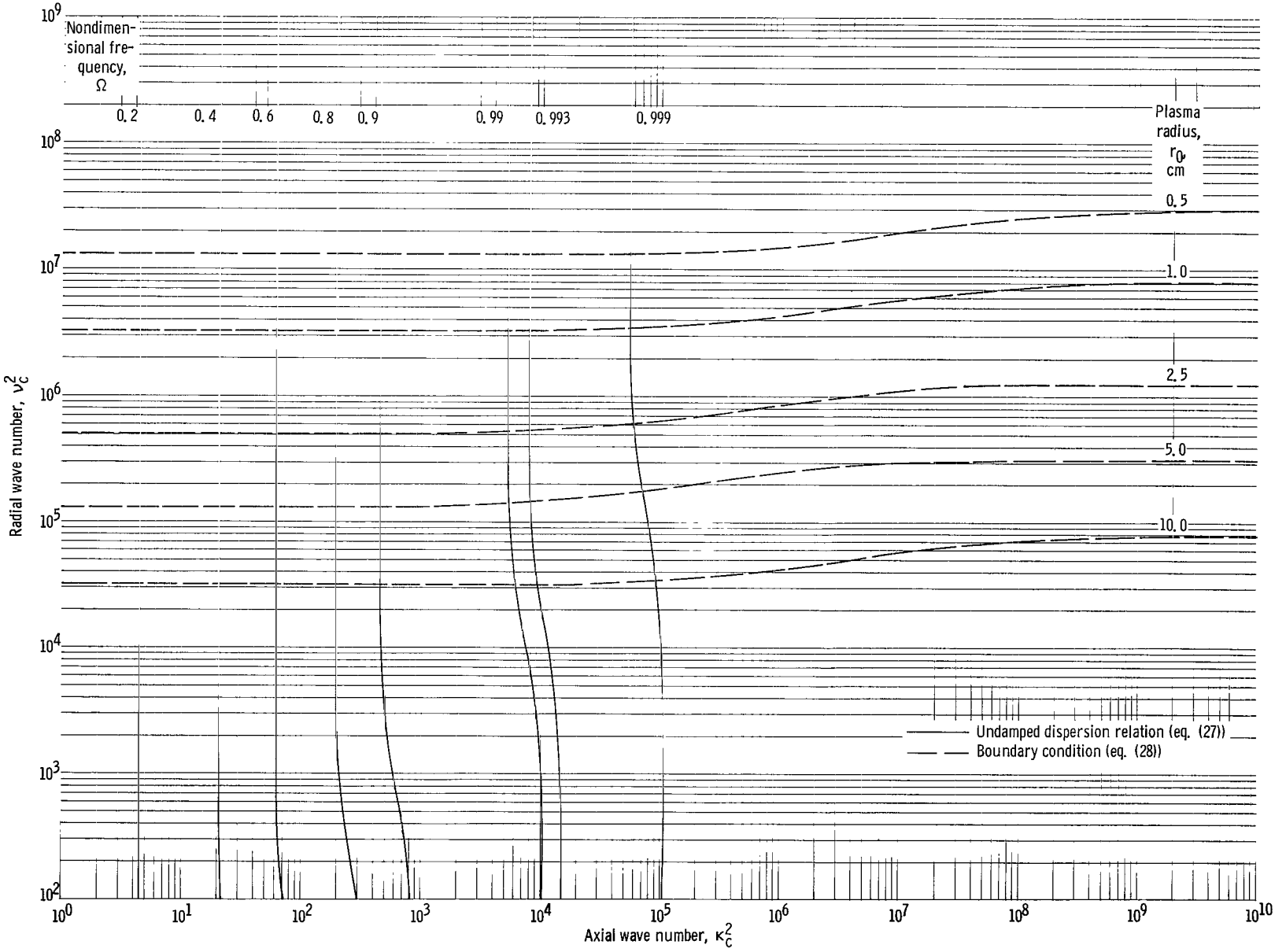

(b) Plasma radii, 0.5, 1, 2.5, 5, and 10 centimeters; mode 1.

Figure 2. - Concluded.

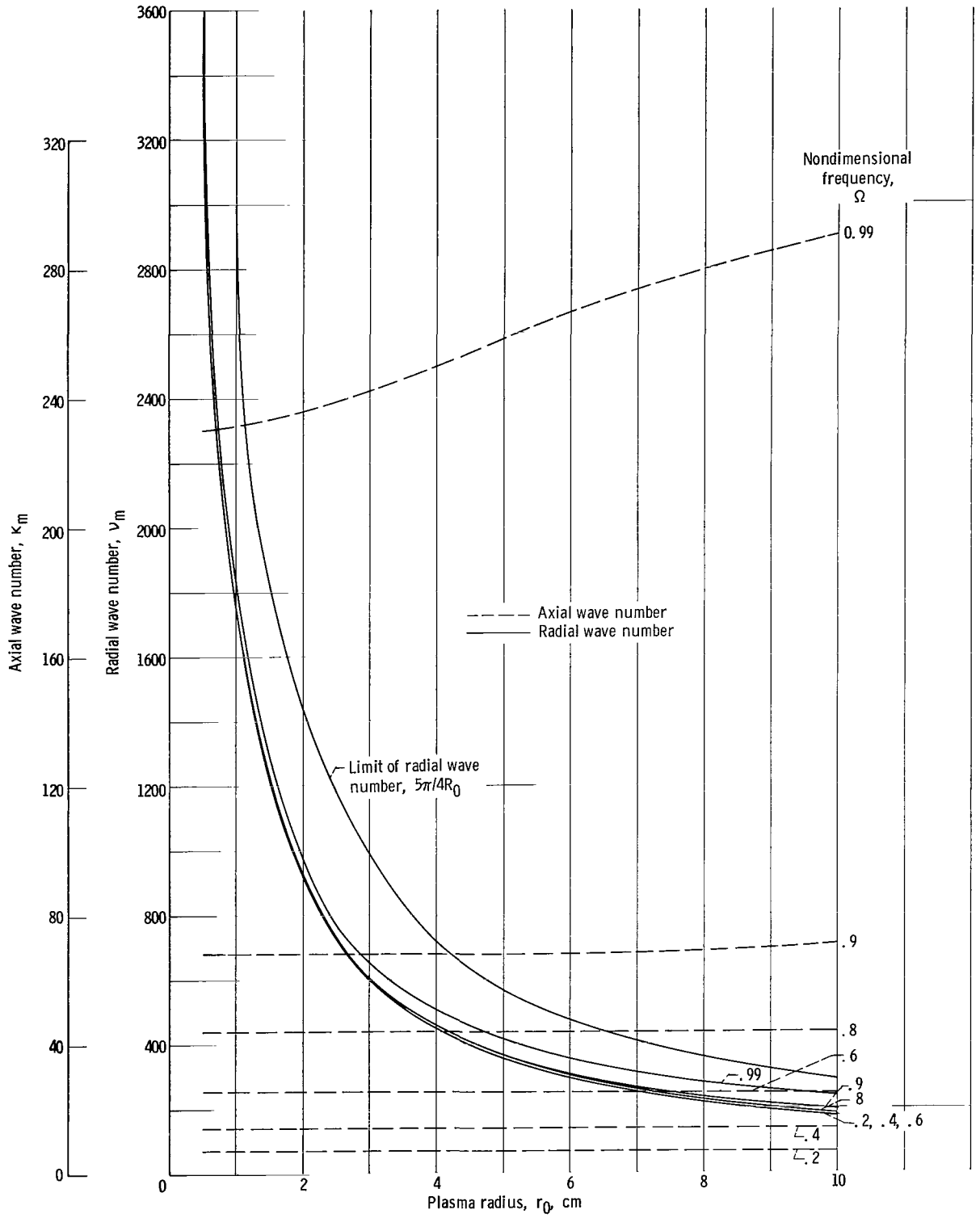

(a) Particle density, 10^{12} ions per cubic centimeter.

Figure 3. - Natural mode wave numbers for cylindrical plasma as function of radius and frequency. Magnetic field, 4.2×10^3 gauss.

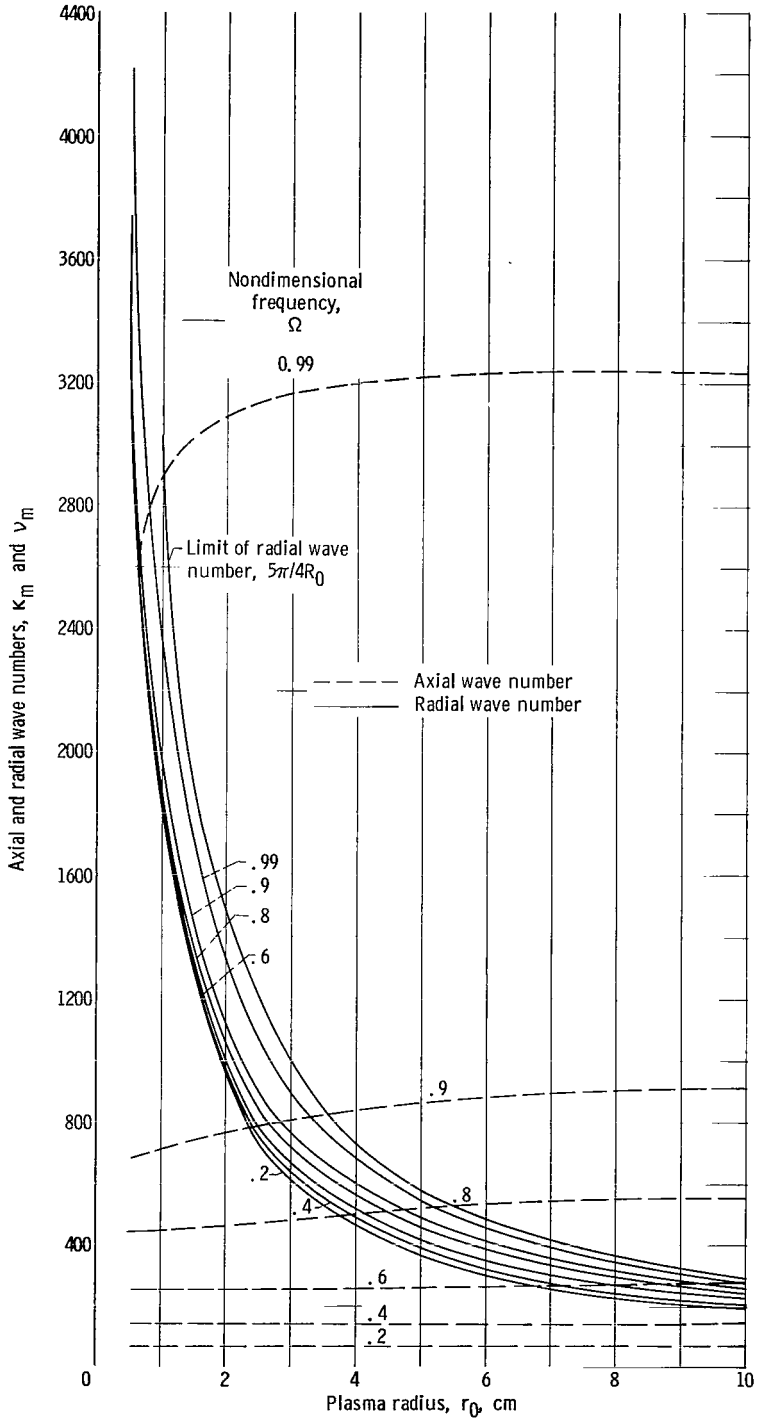

(b) Particle density, 10^{14} ions per cubic centimeter.

Figure 3. - Concluded.

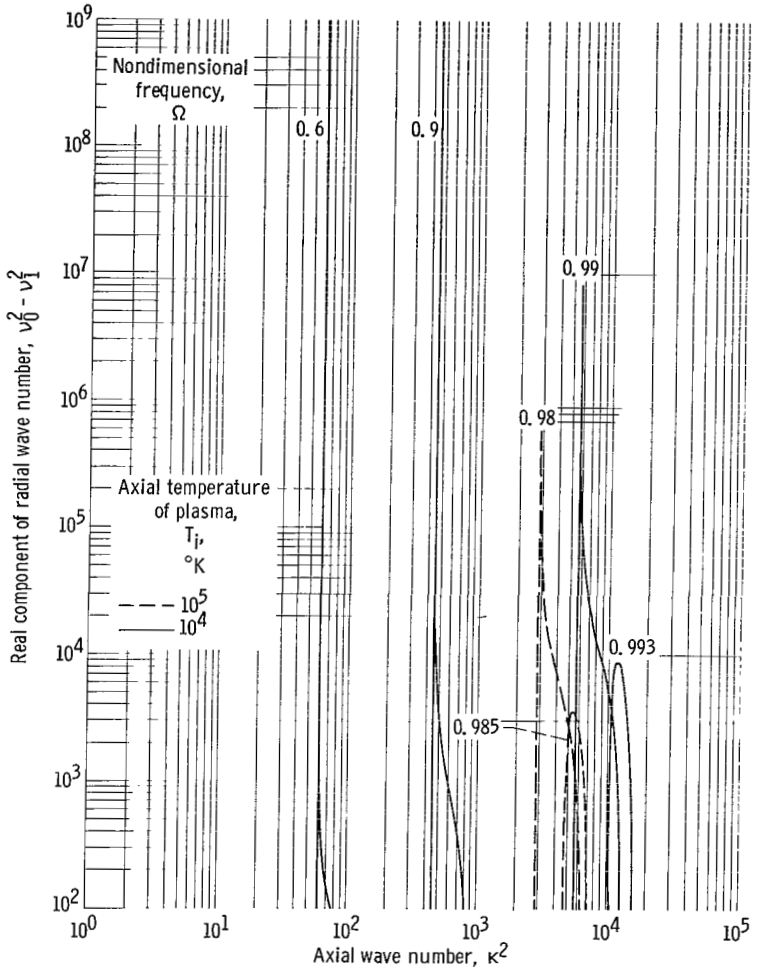

Figure 4. - Dispersion relation for a forced axial distribution including effect of cyclotron damping. Particle density, 10^{11} ions per cubic centimeter; magnetic field, 4.2×10^3 gauss.

the same. It can also be noticed that although the quantity $\nu_0^2 - \nu_1^2$ approximates the nondamped expression closely, there is a difference in the expressions for values of Ω close to 1. The effect of the damping process becomes more and more dominant as the frequency approaches closer and closer to unity. The first major difference for $T_i = 10^4\ ^oK$ is noted at $\Omega = 0.993$, and for $T_i = 10^5\ ^oK$ at $\Omega = 0.985$. Above these frequencies but for Ω still less than 1, the peak of $\nu_0^2 - \nu_1^2$ rapidly decreases and becomes negative.

Absorption Characteristics

Two different power absorption factors were determined: those associated with the

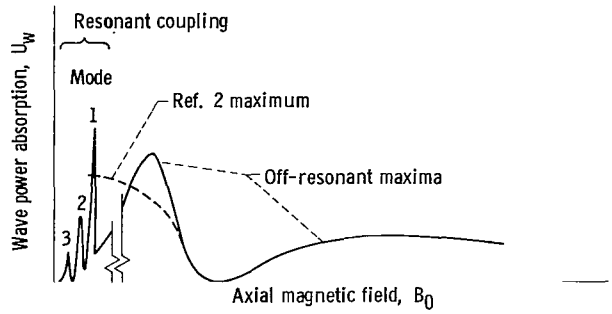

Figure 5. - Schematic of general characteristics of wave power absorption factor.

wave energy of the various plasma modes $(U_w)_m$ and those associated with particle energy U_p. The total wave energy escaping from the coil is the sum of the energies of all the individual modes present. For this report, however, only wave energies of the first three modes were added. This sum is represented as U_w, so that

$$U_w = (U_w)_{m=1} + (U_w)_{m=2} + (U_w)_{m=3}$$

The general characteristics of U_w observed from the present calculations are shown as a function of B_0 in figure 5. The first three peaks measuring from the left represent the coupling resonance for each of the three modes. The scale of B_0 in this region is greatly enlarged (about 50 times). These maxima occur (see eq. (36)) when $\nu_o \approx \nu_m$. The fourth and fifth peaks in figure 5 do not occur near any resonant conditions and therefore are referred to as off-resonant maxima. They originate from that factor of the expression (34) represented by $\left(\frac{\kappa - \kappa_m}{\nu^2 - \nu_m^2}\right)S_0$. The peaking is actually a beat phenomenon (ref. 5, p. 98) developed between the forced and natural modes (see eq. (29)) that exist under the coil.

This description differs from that presented in references 2 and 5, wherein it was assumed that the resistive plasma loading does not vary appreciably near the wave resonant condition. When such an assumption is made the general shape of the U_w curve is similar to the dotted line in figure 5. Consequently, references 2 and 5 predict a wave resonant maximum of large breadth whereas the analysis presented herein predicts several extremely narrow wave resonances along with a medium-width off-resonant maximum. The narrow wave resonant condition is slightly shifted to the right from the resonant condition of reference 2 by a Doppler effect. The off-resonant peak, however, is considerably displaced from the reference 2 maximum.

It is not obvious from the equation for the particle U_p-factor (eq. (21)) that maxima will occur at all B_0 fields where some natural-mode axial wavelengths equal the wavelength of the coil. However, plotting U_p at high T_i does show this characteristic, as depicted in figure 6. The three peaks are associated with the three natural wave modes indicated in figure 5. The displacement of the maximum from $\Omega = 1$ includes the Doppler effect associated with moving particles. Increasing the values of T_i increases this Doppler effect and consequently increases the displacement. When $\Omega \approx 1$, however, cyclotron damping may become so strong that the energy associated with particle motion

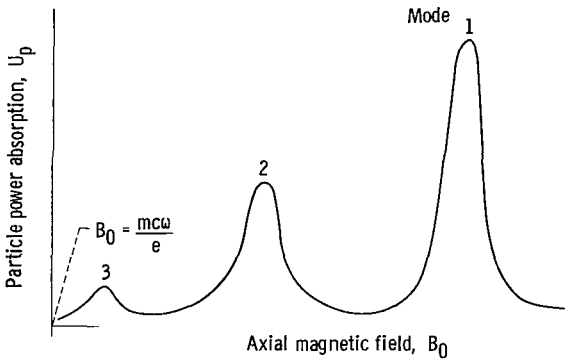

Figure 6. - Schematic of general characteristics of particle power absorption factor.

is essentially "damped" out. The term cyclotron damping, as in reference 2, is associated with the radial flow of energy. The damping modifies the plasma currents in such a way as to reduce the magnitude of the transverse electric fields. Since particle velocity depends on the size of the fields, kinetic energy will also decrease along with the wave amplitude. At these conditions, figure 6 would not be typical of the U_p plots. Near the couple resonant condition the curves of U_p are quite similar to the curves of U_w; each generally exhibits maxima at the couple resonant points. However at larger magnetic fields U_p is very small, whereas U_w is generally significant. This small value of U_p indicates that very little energy is transferred to the particles at the off-resonant maxima.

To investigate the U-factors in more detail, the results of the actual calculations must be examined. Since the steady-state magnetic field strength is the primary variable in most cyclotron-resonance plasma experiments, the U-factor plots were calculated and are presented as functions of magnetic field. A general description of the flow diagram for the program used to calculate the U-factor is presented in appendix B.

Because of the interest in comparing the present results with previous work, all the plots start at a magnetic field consistent with the cold plasma coupling resonant condition determined from the following dispersion relation (eq. (26) of ref. 2):

$$\Omega^2 = \frac{1}{1 + \frac{\alpha}{\kappa^2}} \tag{37}$$

where $\alpha/\kappa^2 = 0.5\times10^{-16}n\lambda^2$, as given by equation (10) of reference 2, and where $\Omega = \omega/(B_0 e/mc)$. At the coupling resonant condition λ, the wavelength of the natural mode is equal to the wavelength of the coil. At this condition, the magnetic field will be referred to as $B_0(\text{res})$, which is generally set at 4.2×10^3 gauss. The frequency given by equation (37) for $B_0(\text{res})$ will be referred to as $\Omega(\text{res})$. Once the magnetic field for coupling resonance is selected, the dimensional frequency can be calculated from equa- (37). Consequently, the parameters n, $B_0(\text{res})$, l, and $\Omega(\text{res})$ appearing in each plot satisfy equation (37).

It was noticed during the calculations that quite frequently negative U_w-factors occurred at magnetic fields somewhat smaller than the fields associated with the couple resonant condition. This would suggest a plasma wave radiating energy to the coil and

therefore would require an additional mechanism to the ones being investigated just to sustain its existence. This added complexity was not considered herein, and regions of negative U-factors were not plotted.

Wave absorption (U_w-factor). - The U_w-factor plots for a coil length of 80 centimeters and for particle densities of 10^{11}, 10^{12}, and 10^{14} ions per cubic centimeter are presented in figure 7. Since the phenomena of coupling resonance occur in regions so small that meaningful data cannot be obtained from plots including both resonant and off-resonant peaks, the data for the two effects are presented separately. Figures 7(a), (b-1), and (c-1) present the data for the off-resonant part of the U_w-factor for particle densities of 10^{11}, 10^{12} and 10^{14}, respectively. Figures 7(b-2) and (c-2) present the data for the coupling resonance for densities of 10^{12} and 10^{14}, respectively. There is no resonant curve for 10^{11} since the effect is damped out at these densities and frequencies. By comparing the location of the maxima of the various curves presented, the trends of the peaks as a function of density may be obtained. However, since the Ω corresponding to resonance changes with the density (eq. (37)) and since $B_0(\text{res})$ remains unchanged in the various curves of figure 7, ω is different for plots with different densities.

The effect of density on the location and the magnitude of the various maxima is portrayed more directly in figure 8. Here the dimensional frequency ω is kept constant and $B_0(\text{res})$ is permitted to vary. In figure 8(a) the location of the first and second off-resonant peaks is shown together with the location of the resonant peak as given by reference 2. The resonant maximum calculated herein would fall in the narrow region between the curve from reference 2 and that for the first off-resonant maximum. All three curves are of similar shape, increasing monotonically with density in the range considered. It would be difficult to determine which curve was being observed experimentally. The difficulty is further aggravated because the half breadth of the resonant peaks is generally much smaller than that of the off-resonant peaks. Conceivably the former would not even be observed. Although the half breadth generally cannot be determined from the results, the actual width of the resonance is what is significant. In almost all cases investigated (which covered a range of particle densities from 10^{11} to 10^{14} ions/cm^3, a range of magnetic fields from 10^3 to 10^5 G, and various coil lengths of 40 to 100 cm), the width of the first maximum was of the order of 5 gauss or less. Nonuniformities in density and the steady-state magnetic field, along with various dissipative phenomena, however, could decrease the magnitude and broaden the width of the resonance. With such conditions present, the couple resonance could become observable. The relative magnitudes of the peaks are shown on figure 8(b). The first and second off-resonant peaks exceed in magnitude the resonant maximum from reference 2. The resonant maximum calculated herein is not shown even though its magnitude would

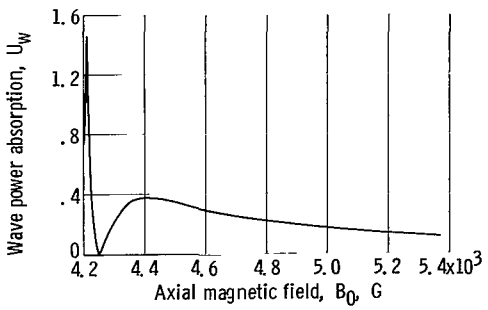

(a) Particle density, 10^{11} ions per cubic centimeter; frequency for value of magnetic field for which coupling resonance of reference 2 occurs, 0.99549; off-resonant maxima.

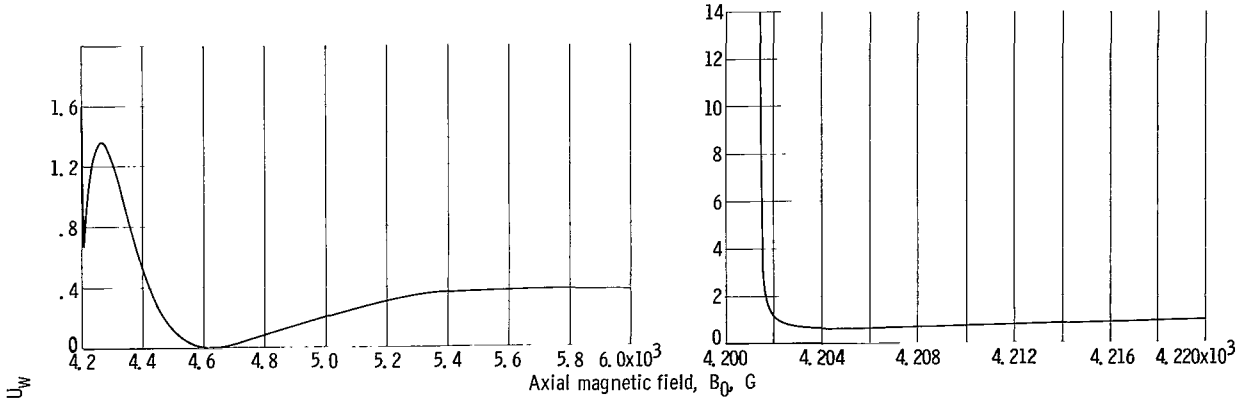

(b-1) Off-resonant maxima.

(b-2) Resonant maxima.

(b) Particle density, 10^{12} ions per cubic centimeter; frequency for value of magnetic field for which coupling resonance of reference 2 occurs, 0.96037.

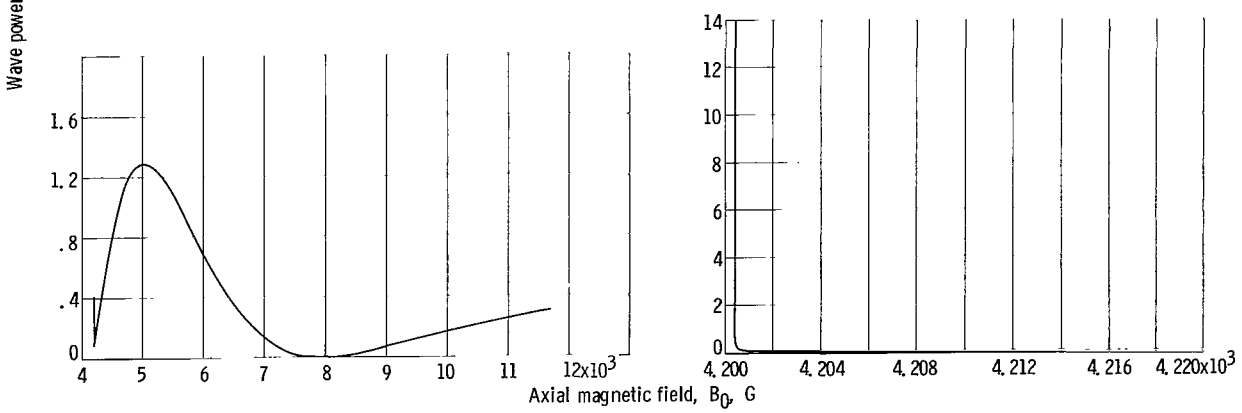

(c-1) Off-resonant maxima.

(c-2) Resonant maxima.

(c) Particle density, 10^{14} ions per cubic centimeter; frequency for value of magnetic field for which coupling resonance of reference 2 occurs, 0.33533.

Figure 7. - Wave U-factor as function of magnetic field for various plasma densities. Magnetic field for which coupling resonance of reference 2 occurs, 4.2x10^3 gauss; coil length, 80 centimeters; plasma radius, 5.0 centimeters; axial temperature of plasma, 10^4 °K.

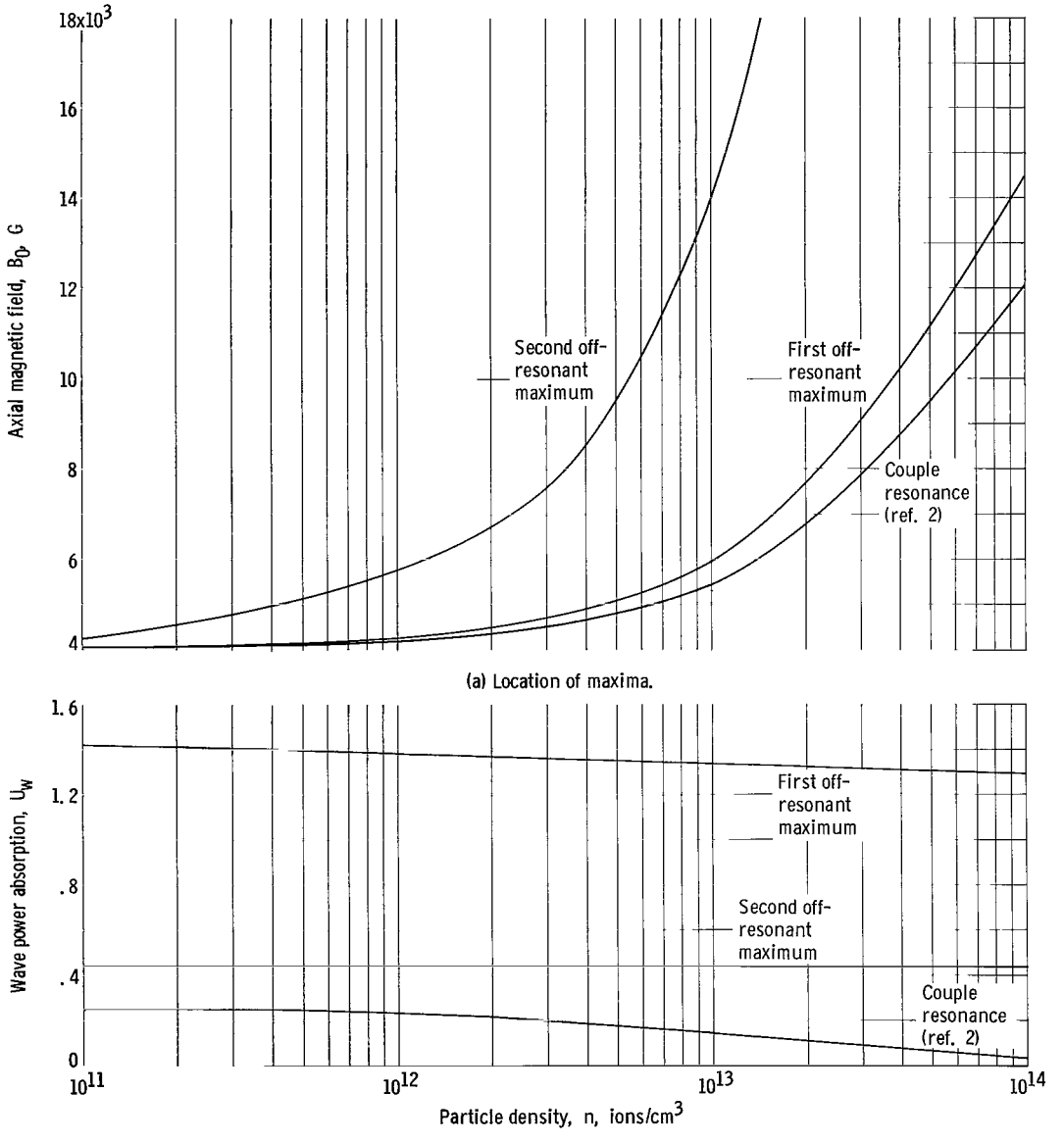

Figure 8. - Characteristics of maximum efficiency as functions of particle density. Frequency, 3.86×10^7 radians per second; coil length, 80 centimeters; plasma radius, 5 centimeters; axial temperature of plasma, 10^4 °K.

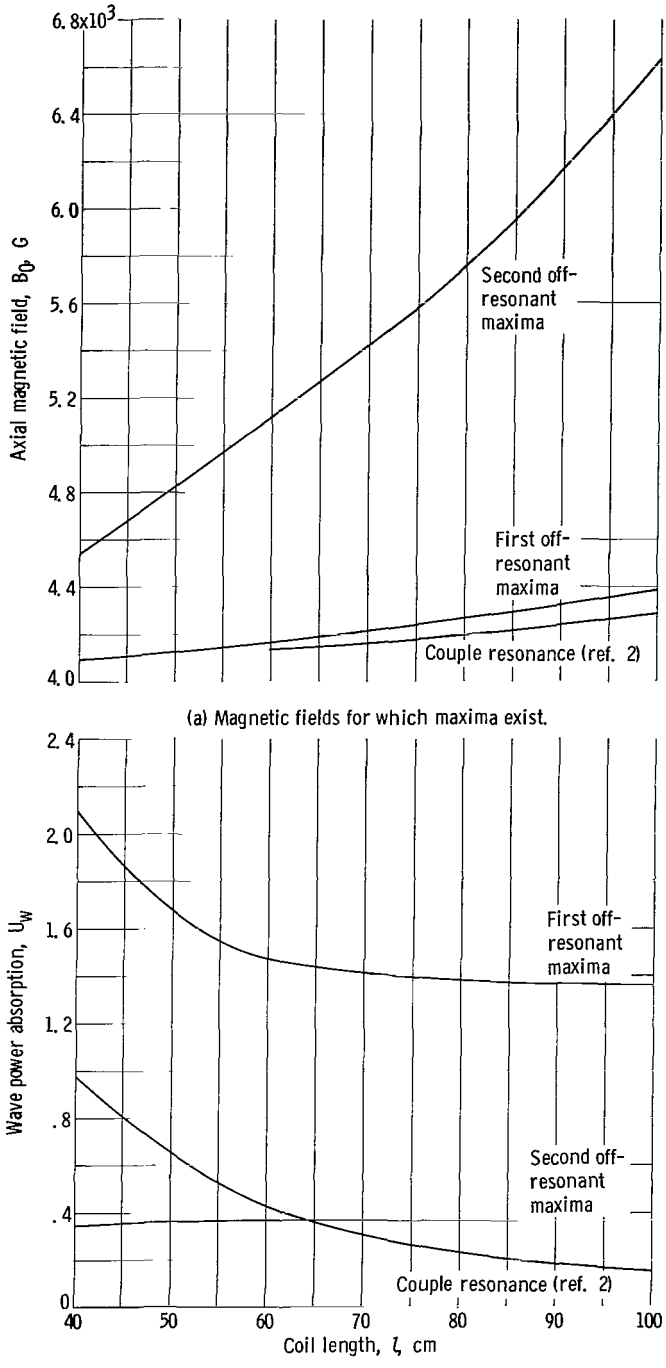

Figure 9. - Maximum U-factors as function of coil length. Frequency, 3.8×10^7 radians per second; particle density, 10^{12} ions per cubic centimeter; axial temperature of plasma, 10^4 °K; number of wavelengths per coil length, 2.

exceed the others. Its previously discussed narrowness limits its significance in a real plasma.

The U-factors for coil lengths of 40, 60 and 100 centimeters were also investigated. Since the general shape of the curves is similar to the data for a coil length of 80 centimeters, however, only the location and magnitude of the off-resonant maximum and the couple resonance peaks of reference 2 are presented in a summary plot (fig. 9). Here again the dimensional frequency ω is constant at the same value as in figure 8. It can be seen from figure 9(a) that there is a very small shift in the first off-resonant maximum as the coil length increases. This shift is quite similar to that calculated from reference 2. A larger effect, though still relatively small, is the decreasing magnitude of the U_w of the first off-resonant maximum as the coil length increases (fig. 9(b)); the U_w-factor drops roughly 30 percent as l increases from 40 to 100 centimeters. Although the magnitude of U_w calculated from reference 2 is considerably less than that calculated for the first off-resonant maximum, the two U_w-factors plotted as a function of l do parallel each other for the l range investigated (fig. 9(b)).

One of the parameters of the system that is difficult to determine experimentally is the plasma radius. The radius used to calculate U_w up to now has been 5 centimeters. To

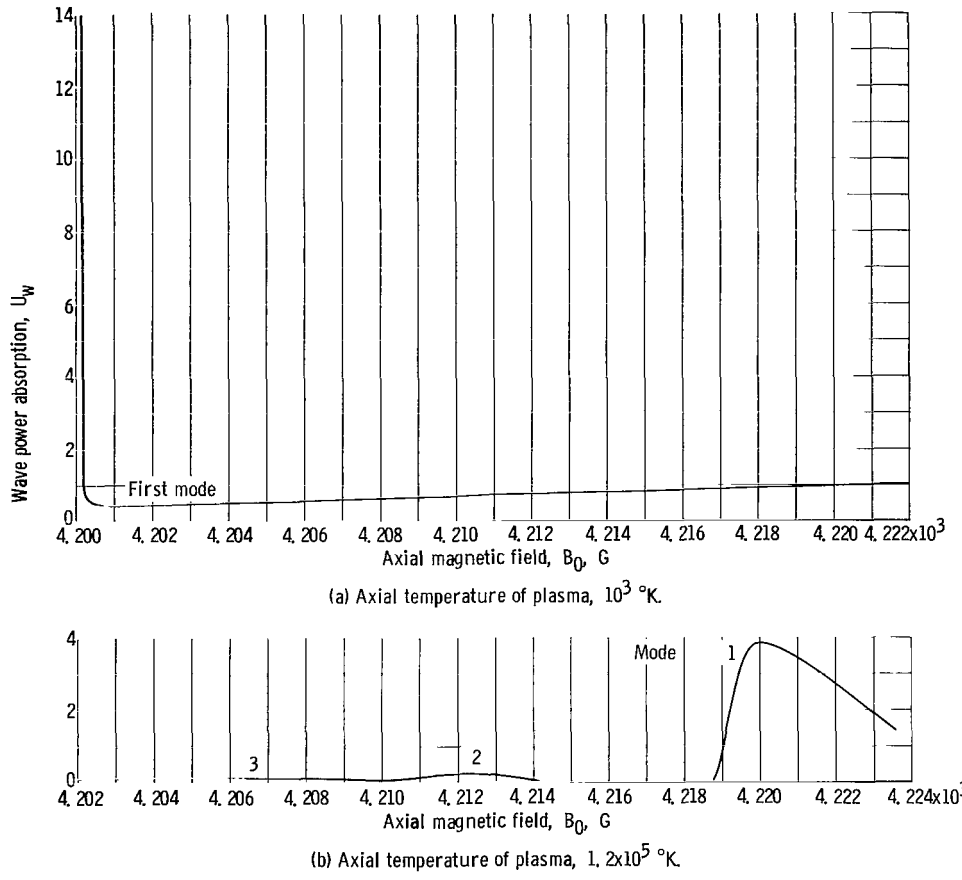

Figure 10. - Wave U-factor of couple resonance as function of magnetic field and axial ion temperatemperature. Particle density, 10^{12} ions per cubic centimeter; magnetic field for which coupling resonance of reference 2 occurs, 4.2×10^3 gauss; frequency for value of magnetic fields for which coupling resonance of reference 2 occurs, 0.96037; coil length, 80 centimeters; plasma radius, 5 centimeters.

ascertain the effect on efficiency, U_w calculations were also made for plasma radii of 0.5, 1.0, 2.5, and 10.0 centimeters at $B = 4.2 \times 10^3$ gauss and $n = 10^{12}$ ions per cubic centimeter. The results indicate that as the radius increases from 0.5 to 10 centimeters, the U_w-factor of the first off-resonant maximum increases from 1.28 to 1.47. Although the effect of a reasonable change in radius is not large, the results do suggest that the plasma should be as big as possible for the most efficient power transfer. The calculations, of course, assumed that the coil radius remained equal to the plasma radius. If the coil radius increases for a fixed plasma radius, there is an additional loss in efficiency that has not been considered, that is, the volume effect of tying up field energy between the plasma and the coil. This does not contribute in any way to the energy added to a plasma but only requires more current in the coil circuit in order to compare cases of equal electric fields at the plasma surface. Consequently, there results an increased I^2R loss.

It can be seen by examining a large number of calculations that the U_w-factors in

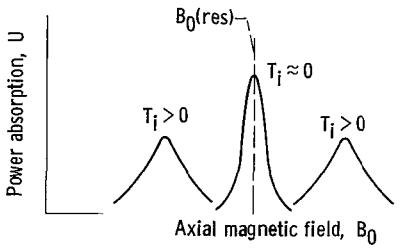

Figure 11. - Schematic demonstrating Doppler effect on power absorption factor near coupling resonance.

the region of the off-resonant maxima are not significantly affected by varying the axial temperature; in fact, the magnitude and location of both off-resonant maxima remain constant. There is a temperature effect, however, on the couple resonance. If such effects are not damped out completely, then a variation in streaming velocity of the ions will modify the shape and location of the couple resonant maximum. This is demonstrated by comparing the first mode maximum in figure 10(a), which occurs at roughly 4.2×10^3 gauss, with the first mode maximum in figure 10(b), which occurs at 4.22×10^3 gauss. This shift is similar to the Doppler shift depicted in figure 11. The two symmetric peaks for $T_i > 0$ represent the Doppler frequency shift corresponding to $\omega \pm kV_z$ (see eqs. (3) and (4) of ref. 2). Because of the strong cyclotron damping effects in the neighborhood of $\Omega = 1$, however, the left member does not always appear. At a density of 10^{11} where $\Omega \approx 0.996$, the damping is so strong at $T_i = 10^4\ ^oK$ that even the right-hand member does not appear. Figure 12 presents the calculated shift of the natural mode resonance along with a simplified Doppler shift which was determined from the expression

$$(\Delta B_0) = \frac{ks_0 mc^2}{e\Omega(res)}$$

It can be seen that the two calculations do not agree. The displacement of the first mode coupling resonance was much smaller than that calculated by the simplified expression. At $10^5\ ^oK$, the displacement was less than one-fifth of that from the simplified equation.

In any case, an interesting observation may be made. If a cold plasma is to be heated to high temperatures at resonant coupling conditions, it may become necessary to adjust the system to stay in resonance as the plasma is heated. As pointed out previously, operation at an off-resonant peak would be less affected by changing temperatures.

Particle absorption (U_p-factor). - When the particle absorption factor U_p and the wave absorption factor U_w are compared, it is recalled that the fields used for the two factors are determined from different models.

The variation of the particle energy with respect to the magnetic field is quite similar, near the couple resonant condition, to the variation of the wave energy. Whenever a coupling resonant maximum appears in U_w there is a corresponding maximum in U_p. Consequently, U_p is generally very sensitive to variations in B_0 in the vicinity of the couple resonant condition. Whenever the coupling resonant effects are negligible or non-

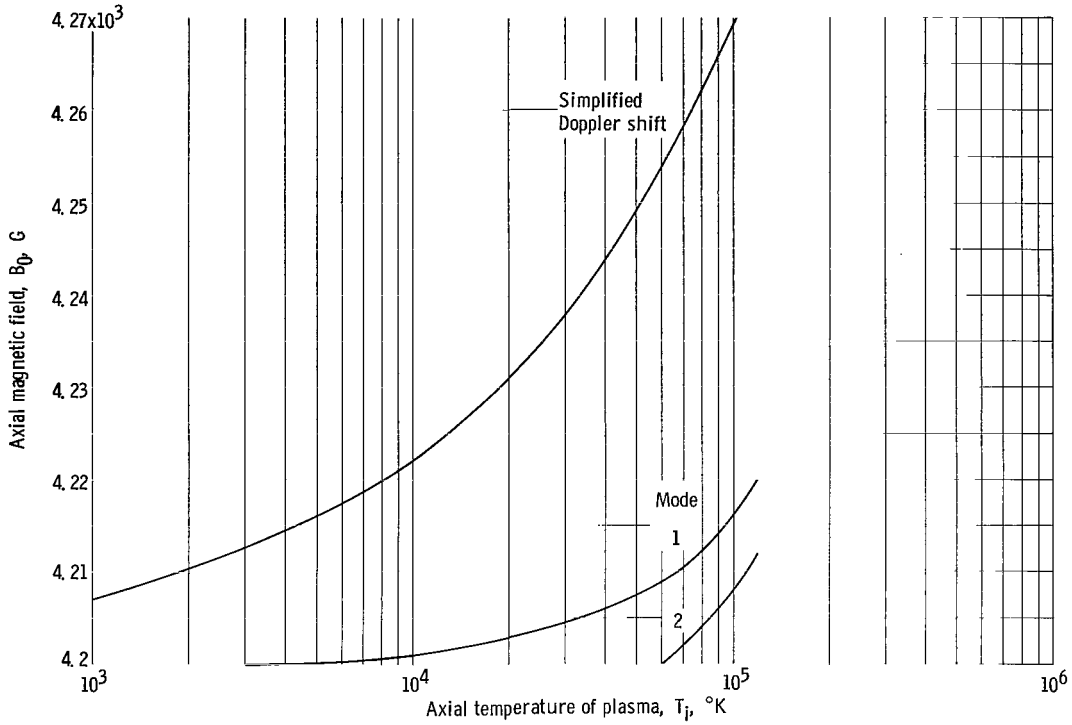

Figure 12. - Location of couple resonance as function of axial temperature. Particle density, 10^{12} ions per cubic centimeter; magnetic field for which coupling resonance of reference 2 occurs, 4.2×10^3 gauss; frequency for value of magnetic field for which coupling resonance of reference 2 occurs, 0.96037; coil length, 80 centimeters; plasma radius, 5 centimeters.

existent in one energy, there is generally a corresponding result with the other energy. Consequently, whenever the couple resonance wave is totally damped, the particle absorption also becomes negligible.

The particle resonance also depends strongly on the particle axial temperature, just as the U_w-factor does. These latter results are depicted in figure 13 in a very expanded scale for the conditions of $B_0(\text{res}) = 4.2 \times 10^3$ gauss, $n = 10^{12}$ ions per cubic centimeter, and for $T_i = 4 \times 10^4$, 6×10^4, 8×10^4, 10^5, and 1.2×10^5 °K. This figure shows that as the axial velocity of the ions decreases (lower streaming temperature), the magnitude of the maxima increases, the half breadth decreases, and their location moves to smaller values of B_0. The half breadths associated with these maxima, however, are generally so small that it would be unlikely that the resonance conditions could be experimentally detected. It should be reemphasized that any conclusions concerning the half breadth of the couple resonance are questionable. Since variations in B_0 are inevitable in an experimental system (even exceeding the half breadth of the peak), the effectiveness of the U_p-factor should perhaps be related to the area under the peaks rather than to their amplitude and half breadths. Consequently, such resonances could possibly be detected. On the other hand, it would probably be unlikely that the large peak magnitudes could actually be realized.

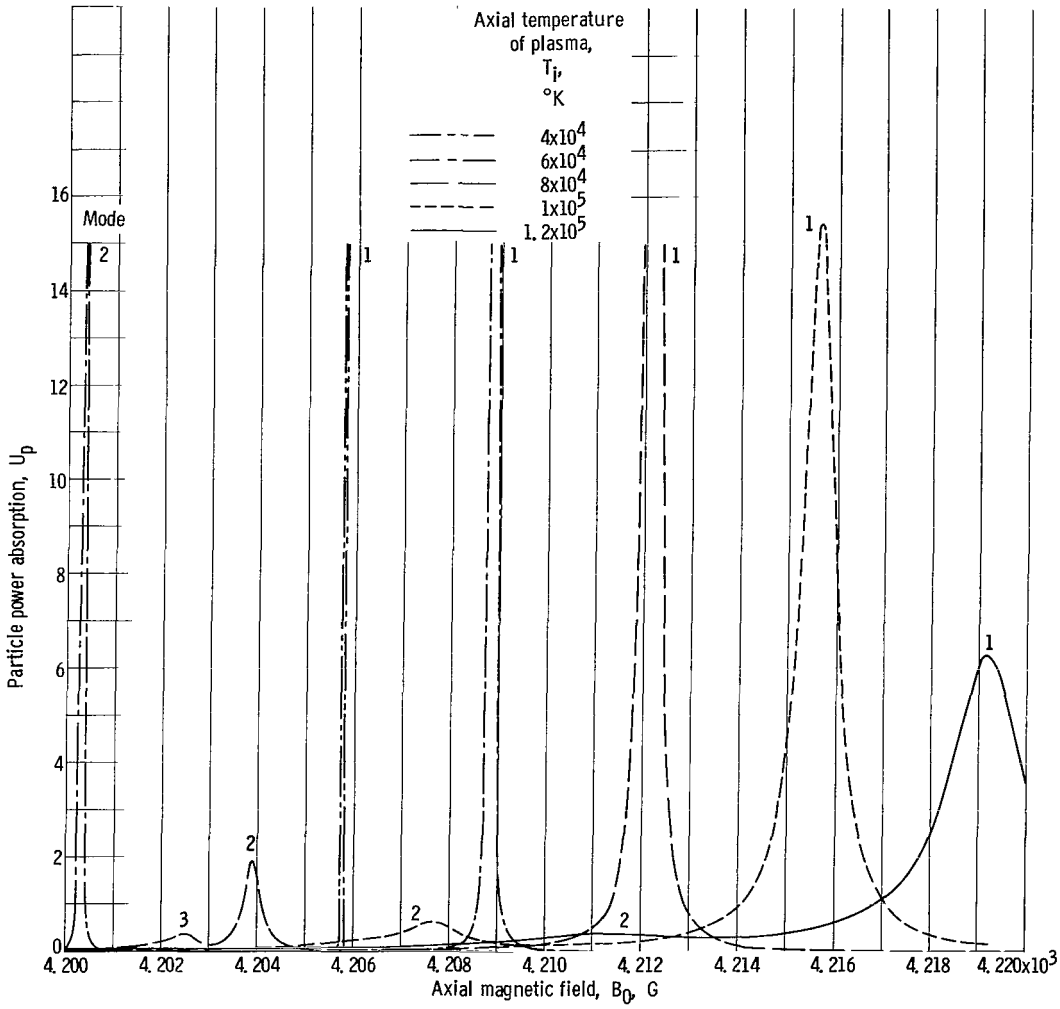

Figure 13. - Particle U-factor as function of magnetic field and axial ion temperature. Particle density, 10^{12} ions per cubic centimeter; magnetic field for which coupling resonance of reference 2 occurs, $4.2x10^3$ gauss; frequency for value of magnetic field for which coupling resonance of reference 2 occurs, 0.96037; coil length, 80 centimeters; plasma radius, 5 centimeters.

At magnetic fields larger than the couple resonant condition, including the fields for the off-resonant peaks of U_w, the particle absorption factor U_p is generally so small in comparison as to be negligible. One exception to this generalization was found in the calculations. This case, which is shown in figure 14, indicates the variation of the U-factors as a function of B_0 for a 40-centimeter coil (λ = 20 cm) at $n = 10^{12}$ ions per cubic centimeter, $B_0(res) = 4.2x10^3$ gauss, r = 5 centimeters, and $T_i = 10^4$ °K. Under these conditions, the location of the first off-resonant peaks for U_w nearly coincides with the location of the couple resonance. This coincidence results principally from the reduction in coil length. As was shown in figure 9, the off-resonant peak moves to lower B_0 fields as the coil length decreases. On the other hand, the coupling resonance for waves at a given temperature shifts to higher B fields as may be seen from the simplified Doppler shift equation. For the case shown in figure 14, both peaks have shifted the

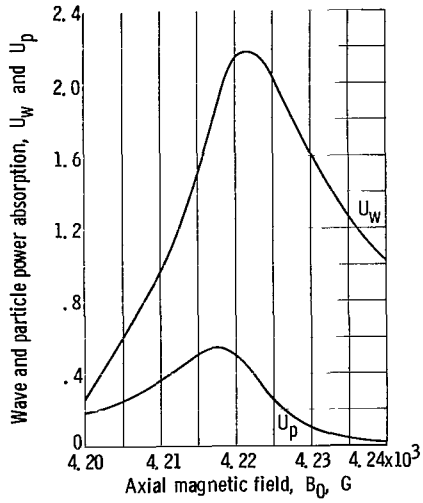

Figure 14. - U-Factor as function of magnetic field. Particle density, 10^{12} ions per cubic centimeter; magnetic field for which coupling resonance of reference 2 occurs, 4.2×10^3 gauss; coil length, 40 centimeters; plasma radius, 5 centimeters; axial temperature of plasma, 10^4 °K.

proper amount so that they will coincide. It should be noted that both absorption peaks are relatively narrow (compare with fig. 7(b)). However, the possibility exists that for some conditions a significant amount of energy could be added to the plasma directly as particle motion, without going through the two-step process of generating and then thermalizing a wave.

CONCLUSIONS

The model used herein to calculate the efficiency of heating a magnetoplasma by the use of a Stix coil is essentially the same as that used in reference 2. However, certain approximations of reference 2 restrict the use of the equation to the coupling resonant condition. In the present case, these approximations are not made. Consequently, the relations developed are applicable off resonance.

The actual power transfer is accomplished by two concomitant processes, the most important being wave generation. Here the Stix coil radiates energy to a cylindrical plasma core, which in turn transmits the wave energy out from under the coil in an axial direction. Accompanying the wave process is an energy addition to the streaming ions. The transverse particle energy is necessary in order to establish the traveling axial waves. When these powers are nondimensionalized and are plotted as functions of the superimposed magnetic field, the resulting curves have sufficient complexity to permit a

more significant comparison with experiment than just the location of a resonance. The following seven characteristics were common to all the response curves.

1. When the power absorption factor (i.e., U-factor) for waves is plotted as a function of the magnetic field, there always exists an off-resonant maximum that appears close to the couple resonant point of the first mode excitation. These additional maxima originate from a beat phenomenon between the forced and natural plasma modes. This new maximum is located on the high magnetic field side of the couple resonant condition. Since this off-resonant peaking has a considerably larger half breadth than the couple resonant half breadth and since it lies so close to it, a possibility exists that it may be mistaken for the coupling condition. The location of the off-resonant peak behaves in a manner similar to the natural mode resonant condition; consequently, a mistaken identity can easily be made which could lead to estimates of density that are large. This description differs from that presented in references 2 and 5 since in these references it was assumed that the resistive plasma loading does not vary appreciably near the wave resonant condition. When such an assumption is made, the wave U-factor monotonically decreases in the region between the wave resonant and the off-resonant maximums, which results in a prediction of a single large breadth maximum.

2. An additional maximum also appeared at magnetic fields larger than the first off-resonant maximum fields. It also originates from a beat phenomenon. The half breadth for this peak, however, is considerably larger than the first off-resonant maximum. Its amplitude is roughly one-third that of the former.

3. Both the first and second off-resonant peaks are insensitive to variations in the plasma size and axial temperature. However, the first off-resonant U-factors for waves did show an inverse wave length sensitivity for the shorter wavelengths.

4. The magnitude of the first and second off-resonant peaks was within an order of magnitude of the couple resonant maxima of reference 2; the first off-resonant peak was always larger.

5. The half breadth of the natural wave resonant maximum was found to be small, so small that it could be difficult to experimentally detect for coil wavelengths greater than 30 centimeters. However, because of nonuniformities in the experimental densities and fields, it is possible that such peaks could be broader than indicated herein. At a small density, where such maxima would be very near the ion cyclotron condition, the couple resonance is completely damped out. As density increases and the resonance moves away from the ion cyclotron condition, less cyclotron damping exists and the maximum is observed.

6. The maxima of particle energy addition occur at the same magnetic field as those of wave energy addition for the natural wave resonances. Particle energy was generally negligible at all other values of field strength even at values where the wave energy peaked at the off-resonant maxima. For a short coil case (coil length, 40 cm), however,

the particle energy was found to be the same order of magnitude as the wave energy at the first off-resonant maximum. This comes about because the couple resonant and the first off-resonant maximum occur at the same field strength.

7. As the axial temperature increases, the "coupling" maxima of the particle U-factor move to larger fields. The half breadth increases and the amplitude of the maximum decreases during this variation.

Lewis Research Center,
National Aeronautics and Space Administration,
Cleveland, Ohio, June 2, 1965.

APPENDIX A

SOLUTION OF EQUATIONS (27) AND (28)

Ordinarily a Newton-Raphson technique would be used to solve equations (27) and (28) simultaneously. However, because the solution of the equations falls extremely close to the singularity of equation (27), that is,

$$-\Omega^2\left[\alpha + (\kappa_c^2 - \Omega_D^2)\right] + (\kappa_c^2 - \Omega_D^2) = 0$$

the correction interval for the first guess could place the second guess on another branch of the curve of equation (27), which would result in a hopeless condition. This difficulty, however, could be circumvented by using a technique that may be considered as an extension of the normal Newton-Raphson equations.

If two new functions ψ and φ are defined using equations (27) and (28)

$$\psi(\nu_c, \kappa_c) = \frac{-\Omega^4\alpha^2 + \Omega^2\left[2\alpha + (\kappa_c^2 - \Omega_D^2)\right](\kappa_c^2 - \Omega_D^2) - \left(\kappa_c^2 - \Omega_D^2\right)^2}{-\Omega^2\left[\alpha + (\kappa_c^2 - \Omega_D^2)\right] + (\kappa_c^2 - \Omega_D^2)} - \nu_c^2$$

$$\varphi(\nu_c, \kappa_c) = -\left(\kappa_c^2 - \Omega_D^2\right)^{1/2} R_0 \frac{K_0\left(\left(\kappa_c^2 - \Omega_D^2\right)^{1/2} R_0\right)}{K_1\left(\left(\kappa_c^2 - \Omega_D^2\right)^{1/2} R_0\right)} - \nu_c R_0 \frac{J_0(\nu_c R_0)}{J_1(\nu_c R_0)} \tag{A1}$$

and if these are expanded in Taylor series

$$\psi(\nu + \Delta\nu, \kappa + \Delta\kappa) = \psi + \Delta\nu \frac{\partial\psi}{\partial\nu} + \Delta\kappa \frac{\partial\psi}{\partial\kappa} + \frac{1}{2}\Delta\nu^2 \frac{\partial^2\psi}{\partial\nu^2} + \Delta\nu\,\Delta\kappa \frac{\partial^2\psi}{\partial\nu\,\partial\kappa} + \frac{1}{2}\Delta\kappa^2 \frac{\partial^2\psi}{\partial\kappa^2} \tag{A2a}$$

$$\varphi(\nu + \Delta\nu, \kappa + \Delta\kappa) = \varphi + \Delta\nu \frac{\partial\varphi}{\partial\nu} + \Delta\kappa \frac{\partial\varphi}{\partial\kappa} + \frac{1}{2}\Delta\nu^2 \frac{\partial^2\varphi}{\partial\nu^2} + \Delta\nu\,\Delta\kappa \frac{\partial^2\varphi}{\partial\nu\,\partial\kappa} + \frac{1}{2}\Delta\kappa^2 \frac{\partial^2\varphi}{\partial\kappa^2} \tag{A2b}$$

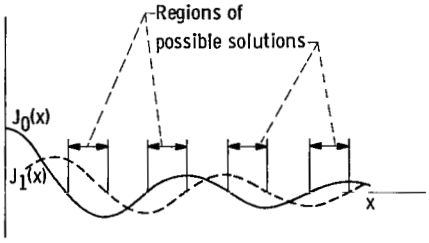

Figure 15. - Schematic of zero- and first-order Bessel functions.

A solution exists when

$$\psi(\nu + \Delta\nu, \kappa + \Delta\kappa) = 0$$

$$\varphi(\nu + \Delta\nu, \kappa + \Delta\kappa) = 0$$

When this latter condition is used, equations (A2) reduce to two algebraic quadratic equations with two unknowns $\Delta\nu$ and $\Delta\kappa$. Eliminating one of the unkonwns, say $\Delta\nu$, results in a quartic equation in $\Delta\kappa$ which must be solved. This can be done quite readily with the use of any one of a number of machine programs. Of the four roots that exist, the one with the smallest absolute value was used in the determination of the correction interval. The values of ν_c and k_c for a solution are designated ν_m and κ_m. The only remaining problem is that of obtaining the first guess of the solution. Equation (28) is some help; since the right-hand side of equation (28) is always negative, the sign of $J_0(\nu_m R_0)$ must always be opposite to that of $J_1(\nu_m R_0)$. Because of the sinusoidal nature of the Bessel functions, the regions of possible solution are values of x between the n^{th} zero of $J_0(x)$ and the $(n + 1)^{st}$ zero of $J_1(x)$. This is graphically demonstrated in figure 15. These factors can be obtained conveniently to any degree of accuracy desired from tables or books on Bessels function. Averaging these two limits will allow the determination of a value of ν_m to be used as a starting point. The companion coordinate κ_m can then be obtained with the use of equation (27) and the starting value of ν_m just mentioned. The modified Newton-Raphson method just described "homes in" on the solution extremely fast, so fast that an answer can many times be obtained after just three or four tries.

APPENDIX B

CALCULATION PROCEDURE

The procedure used to calculate the U-factors was to initially select a plasma density, magnetic field, coil length, and wavelength. A magnetic field of 4.2×10^3 gauss was selected to correspond with current Lewis Research Center experiments (ref. 1). Dimensional frequency was selected to be consistent with (1) the coupling resonant expression of reference 2, (2) the previously indicated magnetic field, and (3) the initial designated parameters. With this dimensional frequency fixed, a variation of the pair (Ω, B_0) can be determined. The natural oscillations of a plasma of a given radius R are then determined for each (Ω, B_0) combination from the simultaneous solution of equations (27) and (28). Before the U-factors can be calculated, the radial wave number of the forced wave must be found from equations (7) and (8). Hence, for a given coil length, a value of ν is found for each (Ω, B_0) pair. Enough information has been assembled at this point to enable the calculation of the U-factors from equations (21) and (36).

REFERENCES

1. Swett, Clyde C.; and Krawec, Roman: Preliminary Observations of RF Power Transfer to a Hydrogen Plasma at Near the Ion Cyclotron Frequency. Proc. Third Symposium on Eng. Aspects of Magnetohydrodynamics, Gordon and Breach Sci. Pub., Inc., 1964, pp. 599-614.

2. Stix, Thomas H.: Generation and Thermalization of Plasma Waves. Phys. Fluids, vol. 1, no. 4, July-Aug. 1958, pp. 308-317.

3. Allis, W. P.; Buchsbaum, S. J.; and Bers, A.: Waves in Anisotropic Plasma. M. I. T. Press, 1963.

4. Shkarofsky, I. P.: Values of the Transport Coefficients in a Plasma for Any Degree of Ionization Based on a Maxwellian Distribution. Canadian J. Phys., vol. 39, no. 11, Nov. 1961, pp. 1619-1703.

5. Stix, Thomas Howard: The Theory of Plasma Waves. McGraw-Hill Book Co., Inc., 1962.

6. Watson, G. N.: A Treatise on the Theory of Bessel Functions. Cambridge Univ. Press, 1944.

7. Miller, W. L.; and Gordon, A. R.: Numerical Evaluation of Infinite Series and Integrals Which Arise in Certain Problems of Linear Heat Flow, Electrochemical Diffusion, etc. J. Phys. Chem., vol. 35, Oct. 1931, pp. 2785-2884.

8. Stix, Thomas Howard: Oscillations of a Cylindrical Plasma. Phys. Rev., vol. 106, no. 6, June 1957, pp. 1146-1150.

3/18/85

"The aeronautical and space activities of the United States shall be conducted so as to contribute . . . to the expansion of human knowledge of phenomena in the atmosphere and space. The Administration shall provide for the widest practicable and appropriate dissemination of information concerning its activities and the results thereof."

—NATIONAL AERONAUTICS AND SPACE ACT OF 1958

NASA SCIENTIFIC AND TECHNICAL PUBLICATIONS

TECHNICAL REPORTS: Scientific and technical information considered important, complete, and a lasting contribution to existing knowledge.

TECHNICAL NOTES: Information less broad in scope but nevertheless of importance as a contribution to existing knowledge.

TECHNICAL MEMORANDUMS: Information receiving limited distribution because of preliminary data, security classification, or other reasons.

CONTRACTOR REPORTS: Technical information generated in connection with a NASA contract or grant and released under NASA auspices.

TECHNICAL TRANSLATIONS: Information published in a foreign language considered to merit NASA distribution in English.

TECHNICAL REPRINTS: Information derived from NASA activities and initially published in the form of journal articles.

SPECIAL PUBLICATIONS: Information derived from or of value to NASA activities but not necessarily reporting the results of individual NASA-programmed scientific efforts. Publications include conference proceedings, monographs, data compilations, handbooks, sourcebooks, and special bibliographies.

Details on the availability of these publications may be obtained from:

SCIENTIFIC AND TECHNICAL INFORMATION DIVISION

NATIONAL AERONAUTICS AND SPACE ADMINISTRATION

Washington, D.C. 20546